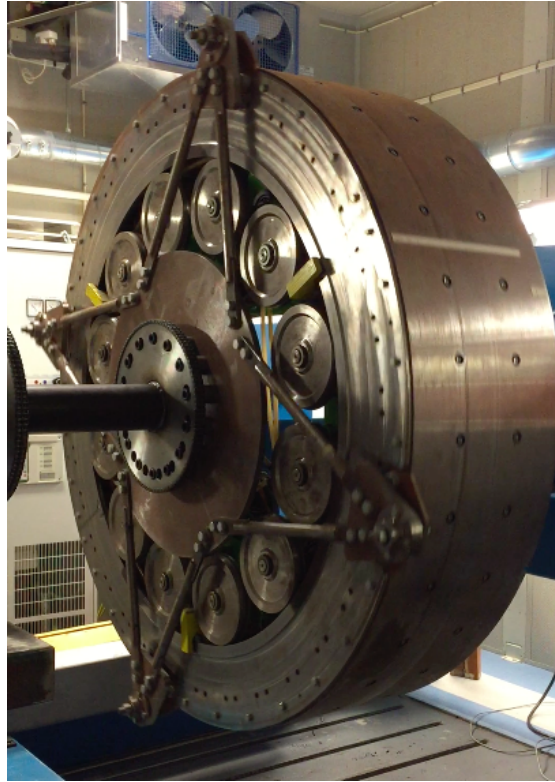




CHALMERS
UNIVERSITY OF TECHNOLOGY



Characterisation and Control of a Permanent Magnet Synchronous Machine during Open Circuit Fault

Master's Thesis in Electric Power Engineering

Erik Ahlqvist & Jonatan Nilsved

Department of Energy & Environment
Division of Electric Power Engineering
CHALMERS UNIVERSITY OF TECHNOLOGY
Gothenburg, Sweden 2015
Master's Thesis 2015

2015

Characterisation and control of a Permanent Magnet Synchronous Machine during Open Circuit Fault

Master's Thesis in Electric Power Engineering

ERIK AHLQVIST
JONATAN NILSVED

Department of Energy & Environment
Division of Electric Power Engineering
CHALMERS UNIVERSITY OF TECHNOLOGY
Gothenburg 2015

Characterisation and control of a Permanent Magnet Synchronous Machine during
Open Circuit Fault
Master's Thesis in Electric Power Engineering
ERIK AHLQVIST
JONATAN NILSVED

© ERIK AHLQVIST
JONATAN NILSVED, 2015.

Department of Energy & Environment
Division of Electric Power Engineering
Chalmers University of Technology
SE-412 96 Gothenburg
Sweden
Telephone +46 (0)31-772 1000

Cover:
Picture of the NewGen mounted in the machine lab at Chalmers.

Teknologtryck
Gothenburg 2015

Characterisation and control of a Permanent Magnet Synchronous Machine during
Open Circuit Fault

Master's Thesis in Electric Power Engineering

ERIK AHLQVIST

JONATAN NILSVED

Department of Energy & Environment

Division of Electric Power Engineering

Chalmers University of Technology

Abstract

This thesis describes a complete setup of an electric driveline consisting of a permanent magnet synchronous machine, PMSM, converter and a control system. In order to model the system, the parameters of the selected machine parameters needed to be characterised. Comparison between the simulations and tests confirmed that the parametrisation was accurate and the system could be operated in both motor and generator mode. Moreover, simulations of an open circuit fault was performed and a resonant controller implemented to reduce the torque ripple which occurred due to the fault. Similar tests was performed in the lab-setup, which confirmed that the machine was able to continue to operate during an open circuit fault using only a PI-controller if the wye node current is controlled. The same resonant controller was implemented in the control system in the lab, however, due to high frequency noise in the current measurements, it became unstable. As a replacement, a look-up table using the output from the simulated resonant controller was implemented which lowered the torque ripple significantly. From this it is concluded that the resonant controller shows very good performance in simulations and would theoretically do so in lab implementation. However, a real implementation is very hard to achieve, even though the look-up table version did lower the torque ripple significantly.

Acknowledgements

First, we would like to thank our supervisor PhD student Joachim Härsjö for the support and good ideas during this thesis. We would also like to thank our examiner Prof. Ola Carlson for ideas and the opportunity to carry this thesis, it has been a pleasure. Last but certainly not least, a special thanks to our better halves, that had put up with us when we needed to spend weekends at school.

Erik Ahlqvist & Jonatan Nilsved, Gothenburg, July 10, 2015

Contents

Abstract	v
Acknowledgements	vii
Contents	ix
1 Introduction	1
1.1 Aim	2
1.2 Problem/Task	2
1.3 Limitations	2
1.4 Method outline	3
2 Theory	4
2.1 PMSM	4
2.1.1 Modeling of PMSM	6
2.2 Converter	11
2.2.1 Faults in Converter	11
2.2.2 Converter Topologies	12
2.3 Controller	13
2.3.1 PI-controller	13
2.3.2 Resonant controller	17
2.4 Pulse width modulation	18
3 Lab setup	19
3.1 NewGen	20
3.2 Controller	20
3.2.1 Real time interface	21
3.3 Position sensor	22
3.3.1 Encoder instalment and calibration	23
3.4 Converter	25
3.5 Current measurement	26

3.6	DC Power Supply	26
4	Machine Characterization	28
4.1	Tests	28
4.1.1	Stator resistance and inductance	29
4.1.2	Flux linkage evaluation	31
4.1.3	Machine damping	31
4.1.4	Inertia	31
4.2	Results and analysis	32
4.2.1	Resistance and inductance measurements	32
4.2.2	Results from Ψ_m evaluation	35
4.2.3	Machine damping results	36
4.2.4	Results from Inertia test	37
4.3	Discussion of results	37
4.3.1	Stator resistance and inductance	37
4.3.2	Flux linkage results	38
4.3.3	Machine damping equation	38
4.3.4	Inertia test	38
5	System simulation	39
5.1	Model setup	41
5.1.1	PMSM	41
5.1.2	Controller	41
5.1.3	Speed controller	42
5.2	Simulations	43
5.2.1	Torque response	43
5.2.2	Three-phase reference	43
5.2.3	Two-phase PI-control	43
5.2.4	Resonant controller	43
6	Experimental test method	44
6.1	Setup	44
6.2	Lab tests	44
6.2.1	Torque response	44
6.2.2	Three-phase reference	45
6.2.3	Two-phase current control	45
6.2.4	Resonant controller	45
6.2.5	Identifying sinusoidal component	46
7	Results	47
7.1	Model verification	47
7.1.1	Simulation	47
7.1.2	Lab verification	48
7.2	Open circuit phase fault	49

7.2.1	Simulations	49
7.2.2	Identifying sinusoidal component	51
7.2.3	Lab tests	51
8	Discussion	53
9	Conclusion	55
9.1	Further research	55
	Bibliography	58
A	Equipment setup	A1
A.1	Test object PMSM	A1
A.2	Induction machine	A2
A.3	Converter	A2
A.4	Gearbox	A2
A.5	dSpace	A3
A.6	Measurement equipment	A3
A.6.1	Position sensor	A3
A.6.2	Oscilloscope	A3
A.6.3	Current sensors	A4
A.6.4	Voltage probes	A4

List of Figures

2.1	Different ways of mounting the permanent magnets on a PMSM with outer rotor.	5
2.2	Simplified three phase representation of the PMSM	8
2.3	Stator current vector from three phase quantities.	9
2.4	Converter topologies	12
2.5	Machine and controller block system	14
2.6	Current regulator design	15
2.7	Closed loop system	16
2.8	Controller with resonant part	17
3.1	Lab setup	19
3.2	dSPACE Hardware	21
3.3	dSPACE Software	22
3.4	Solution to the secondary rotation of the incremental encoder mounting axle.	24
3.5	Difference in position measurement from ideal conditions [mechanical rad].	25
3.6	Regulation of the two different DC sources.	27
4.1	AC standstill test connection.	30
4.2	Main and induced voltages for two different positions and two current levels.	33
4.3	All induced voltages for the two positions.	34
4.4	Measured back-emf for three different speeds.	35
4.5	Torque-speed relation for tested operating points and linear curve fits for different data sets.	36
4.6	Coast down tests for three initial speeds and their fitted exponential curves.	37
5.1	General overview of the system simulated in Simulink	40
5.2	Current controller implemented in simulink	42
5.3	Resonant controller implemented in Simulink	42
6.1	PI controller in Simulink RTI	45

6.2	Resonant controller in Simulink RTI	46
6.3	Introducing the response from the simulated resonant controller.	46
7.1	Simulation of start behaviour, speed reference	48
7.2	Validation of torque response	49
7.3	Simulated behaviour during resonant controller turn on	50
7.4	Simulated behaviour during resonant controller turn on	51
7.5	Behaviour during resonant controller turn on	52
A1	System setup	A1

List of Tables

4.1	Parameters for simulation application	29
4.2	Stator resistance, all results in $m\Omega$	34
4.3	Average values for stator resistance, inductance and mutual inductance.	35
4.4	Back-emf constant values.	36
4.5	Machine damping constant, b , and Coulomb friction, J_0	36
4.6	Machine inertia, J , for each initial speed and the average value.	37
A1	Machine parameters [1].	A2
A2	Induction machine technical data.	A2
A3	Gearbox technical data.	A2
A4	Encoder technical data.	A3
A5	Oscilloscope technical	A4
A6	Current probe.	A4
A7	LeCroy AP032 voltage probe.	A5

1

Introduction

The attempt to reduce the amount of fossil fuels used in the world has led to a significant increase in the use of large electrical machines in the areas of transportation/automotives and in power generation. Permanent magnet synchronous machines, abbreviated PMSM, are strong contenders in a wide variety of applications where weight is of importance due to their comparatively high power density, high efficiency and torque-to-inertia ratio. Additionally, they provide high reliability since permanent magnets means less stress on the electrical system. They are a very common choice in automotive propulsion, whether it be hybrid or pure electrical, and are increasingly popular in wind turbines [2, 3].

Due to the synchronous nature of a PMSM a converter is needed for control in order to provide variable frequency and voltage, regardless if the application is as a generator or motor. In an automotive context where the power is provided from a battery a single converter is used, but in wind turbines a back-to-back system with two converters is needed. What the two systems have in common is that the machine side converter is responsible for controlling the machine, whether it be in motor or generator mode. This is done by converting an DC voltage into AC voltage. [4].

Converter failure can have serious consequences. As wind farms tend to be placed at remote locations and can therefore part of the time be inaccessible, maintenance and repairs when faults occur are often difficult and sometimes delayed due to weather conditions or waiting time for spare parts. Depending on the topology of the wind farm a single converter fault could result in the entire farm being out of operation for the duration of the repairs, causing loss of production. This not only results in income losses for the operator but also means the lost production has to come from other, perhaps less environmentally friendly, producers.

In an automotive application, converter failure, could cause the car to be completely stranded with discomfort or even danger as a result for the driver. A converter can fail in many different ways, but anything resulting in the loss of more than one phase will

be impossible to overcome without actual repair being carried out. However, if only one phase is lost the converter could theoretically still be kept in operation.

If the converter could be devised and controlled in a way that allows for two phase operation, even at reduced output, it would mean higher reliability, greater safety on the road and less risk of production loss in power generation.

1.1 Aim

The aim of this master thesis is to operate a Permanent Magnet Synchronous Machine during open circuit fault using a resonant controller.

1.2 Problem/Task

The main tasks of this thesis is firstly to investigate the behaviour of the NewGen Permanent Magnet Synchronous Machine during one phase open-circuit fault. Secondly, simulate and control the machine during fault using a PI-controller. Furthermore, simulate and investigate if the fault operation can be improved by the implementation of a resonant controller. The computer simulations will be performed in advance of the lab tests in order to verify the theorised control methods. The subtasks needed to fulfill the main goal are:

- Characterise the machine parameters needed to model the machine.
- Develop a simulation model that closely mimics the behaviour of the system.
- Modify a controller to handle one phase open-circuit fault.
- Introduce one phase open circuit faults to the converter used to control the machine.
- Simulate the use of a resonant controller during open-circuit fault and evaluate whether it is able to reduce current ripple further than what is accomplished by the original PI controller.
- Test the simulated solution in the lab setup and evaluate its effect on overall current ripple and stability.

1.3 Limitations

Many different fault conditions can occur in a three phase converter during operation, this thesis focuses only on open circuit fault in a single leg of the converter and errors that originate thereof.

The individual parts of the drive system is inherited and will not be changed, thus the focus will be on system implementation and control of this particular system.

1.4 Method outline

Firstly a literature study in the relevant areas was performed. Specifically PMSM machine characterisation, mechanical and electrical PMSM modelling, controller theory, three phase converter theory, converter fault cases and the current research regarding one phase open circuit faults.

The machine characterisation consisted of four main tests intended to acquire the parameters needed for machine control and modelling for simulations. Parallel to the characterisation a SimuLink model of the system was created including a machine model and a converter for speed and torque control. In order to perform the last two characterisation tests the PMSM was used in motor mode and controlled using a converter. The controller was written in C-code and implemented using dSpace.

The validity of the Simulink model created and the parameters found through the characterisation was tested by comparing the behaviour of the model to that of the PMSM during acceleration to a set speed.

The next step was to simulate one phase open circuit faults in the converter and observe what difficulties this might cause for the real system. Furthermore, adding a resonant controller to the standard PI-control to reduce the noise and instability that occurred due to the phase fault.

Using the knowledge gained from the simulations the dSpace controller was modified to handle open circuit faults, using only its original PI-control. For easier implementation and configuration a new controller using Simulink to dSpace conversion was created. The modifications included using one of the converters legs to control the zero current, allow relatively smooth two-phase operation.

Finally the resonant controller was implemented in the Simulink-dSpace controller.

2

Theory

The following chapter contains the machine and controller theory that is the basis of the method used.

2.1 PMSM

A PMSM is an electrical machine in which the rotor excitation field is provided by permanent magnets instead of being induced by feeding current through windings. The stator is constructed in a similar way as in AC induction machines.

In later years the use of PMSM's in wind power applications have become more prevalent due to their high efficiency and robustness. Since they do not need a system to provide a rotor current they require less maintenance than, e.g. doubly fed induction generators, DFIG. Furthermore, PMSM's can be used without a gearbox, resulting in lighter total hub weight and higher dependability [5].

Since the PMSM has a constant magnetic field, the frequency of induced voltage is equal to the electrical speed of the machine. In order to produce torque, the stator currents must also have the same frequency as the electrical speed of the machine. Using the PMSM without a gear box means the gearing has to be done electrically by selecting an appropriate number of poles that the machine is equipped with allowing it to operate at its optimum for a certain range of wind speeds in a wind power setting [5, 6].

Permanent magnet mounting

There are three main ways of mounting the permanent magnets on the rotor as seen in Figure 2.1. These three methods all influence machine behaviour differently, a machine with surface mounted permanent magnets will have a comparatively simple construction

and will in principle be non-salient, i.e. equal d and q inductance. However, the magnets will not be protected against mechanical stresses. One way to reduce these stresses is to use an interior mounting. This will protect the magnets but results in higher leakage flux. The middle way is to use insets to mount the magnets which will lower the leakage flux and increase the maximum torque capabilities, but with more torque oscillation when compared to interior mounting. Another advantage of surface mounted magnets is that air gap reluctance will be uniform since the reluctance of the magnets is almost equal to that of air. This is not the case for most rotor materials, which means the magnetic coupling will be dependent on rotor position for inset and interior mounting, resulting in cogging torque if not accounted for.[7, 8]

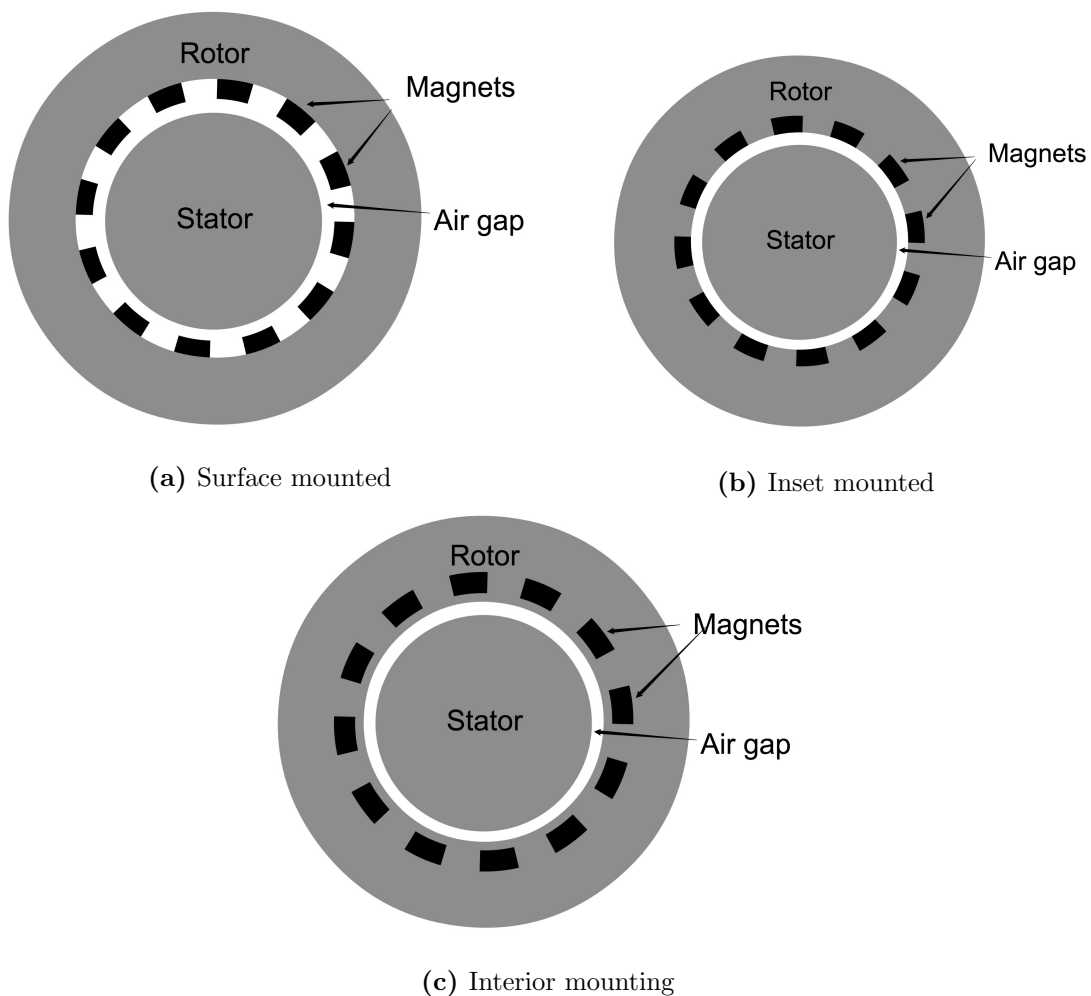


Figure 2.1: Different ways of mounting the permanent magnets on a PMSM with outer rotor.

2.1.1 Modeling of PMSM

Mechanical model

The acceleration of an electrical machine can be described by the following equation,

$$\frac{d\Omega_r}{dt} = \frac{1}{J}(\tau_{em} - \tau_L - b\omega_r - J_0) \quad (2.1)$$

where J is the machine inertia, Ω_r is the mechanical speed, τ_{em} the applied electrical torque, τ_L the load torque, b the mechanical friction and J_0 the Coulomb friction or breakaway friction. This is however a simplified model that has a serious flaw, causing it to be discontinuous at low speed since the Coulomb friction term would seem to drive the machine backwards, which is evidently not the case.

Electrical model

The phase voltage of a PMSM can be expressed as

$$u_s = R_s i_s + \frac{d\Psi_s}{dt} \quad (2.2)$$

where u_s is the phase voltage, i_s is the current in that phase, R_s the phase resistance and Ψ_s is the flux linking the phase. This flux can be expressed as follows for phase a in a three-phase case

$$\Psi_a(t) = \int_0^t (u_a - R_s i_a) dt = (L + L_{\lambda a}) i_a + M_{ab} i_b + M_{ac} i_c + \omega_r \Psi_m \cos(\theta - \varphi_a) \quad (2.3)$$

where L is the self inductance, L_{λ} the leakage inductance, M_{ab} and M_{ac} is the mutual inductance. Ψ_m is the permanent magnet flux linkage, θ is the angle between the reference position and the corresponding magnets north pole. φ_a is the angle between the direction of the magnetic field of phase a and the reference point. If phase a is chosen as the reference point, φ_a will be zero and φ_b and φ_c will be $-\frac{2\pi}{3}$ radians and $\frac{2\pi}{3}$ radians respectively.

The permanent magnet flux linkage is determined by the relation between peak back-emf and electrical speed of the machine,

$$\Psi_m = \frac{\hat{U}_{L-N}}{n_p \omega_r} \quad (2.4)$$

If the phases of the machine are uniform in relation to each other it can be assumed that the mutual and leakage elements of the inductance are independent of phase

$$L_{\lambda a} = L_{\lambda b} = L_{\lambda c} = L_{\lambda} \quad (2.5)$$

$$M_{ab} = M_{bc} = M_{ca} = M \quad (2.6)$$

This means the stator inductance are identical for all phases

$$L_s = L_{\lambda} + L \quad (2.7)$$

As explained in the introduction to chapter 2.1 there are different ways to mount the magnets on a PMSM. This will impact air gap reluctance and thus the rotor magnetic field strength which in turn affects the magnetic flux and inductances. If the machine have surface mounted magnets the impact will be minimal compared to inset mount since the reluctance of the magnets is very close to that of air. Hence, there will be a uniform air gap reluctance and the magnetic coupling will not be dependent on rotor position. If, in addition to this, saturation is neglected the inductance values will not be position or time dependent,

$$\frac{dL_s}{dt} = \frac{dM}{dt} = 0 \quad (2.8)$$

using this and the derivative of (2.3) it is possible to derive a machine model expression for phase a ,

$$\frac{d\Psi_a}{dt} = \frac{d}{dt} \left(\int_0^t (u_a - R_s i_a) dt \right) = \{U_a - R_s i_a\} = L_s \frac{di_a}{dt} + M \left(\frac{di_b}{dt} + \frac{di_c}{dt} \right) - \omega_r \Psi_m \sin(\theta) \quad (2.9)$$

where ω_r is the electrical speed of the rotor and thus the derivative of the rotor position. Extracting U_a gives,

$$U_a = R_s i_a + L_s \frac{di_a}{dt} + M \frac{di_b}{dt} + M \frac{di_c}{dt} - \omega_r \Psi_m \sin(\theta) \quad (2.10)$$

and the three phase model, using phase a as reference, can be expressed in matrix form,

$$\begin{bmatrix} U_a \\ U_b \\ U_c \end{bmatrix} = \begin{bmatrix} R_s & 0 & 0 \\ 0 & R_s & 0 \\ 0 & 0 & R_s \end{bmatrix} \begin{bmatrix} i_a \\ i_b \\ i_c \end{bmatrix} + \begin{bmatrix} L_s & M & M \\ M & L_s & M \\ M & M & L_s \end{bmatrix} \frac{d}{dt} \begin{bmatrix} i_a \\ i_b \\ i_c \end{bmatrix} - \omega_r \Psi_m \begin{bmatrix} \sin(\theta) \\ \sin(\theta - \frac{2\pi}{3}) \\ \sin(\theta + \frac{2\pi}{3}) \end{bmatrix} \quad (2.11)$$

Figure 2.2 displays a simplified circuit representation of the PMSM where the back emf part is present. This voltage is, as explained in chapter 2.1 and shown in (2.11) directly dependent of the speed of the rotor.

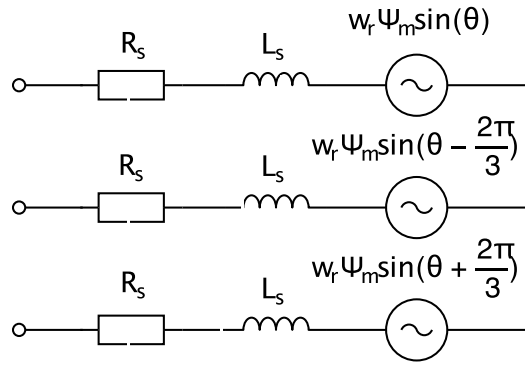


Figure 2.2: Simplified three phase representation of the PMSM

Space vectors

The three phase quantities of an AC-machine can be expressed through complex vectors which can be represented in a Cartesian coordinate system. For a generator system, the chosen coordinate system is grid voltage oriented to allow simplified control.

Due to the difference between phase angle the sum of the three phase currents at any time will be zero in a balanced wye-connected system,

$$i_{sa}(t) + i_{sb}(t) + i_{sc}(t) = 0 \quad (2.12)$$

these currents can be combined to form a vector $\underline{i}_s(t)$, which will rotate with the stator frequency, f_s ,

$$\underline{i}_s = \frac{2}{3}(i_{sa}(t) + i_{sb}(t)e^{j\gamma} + i_{sc}(t)e^{2j\gamma}) \quad (2.13)$$

where $\gamma = \frac{2\pi}{3} = 120^\circ$. This can be seen in Figure 2.3.

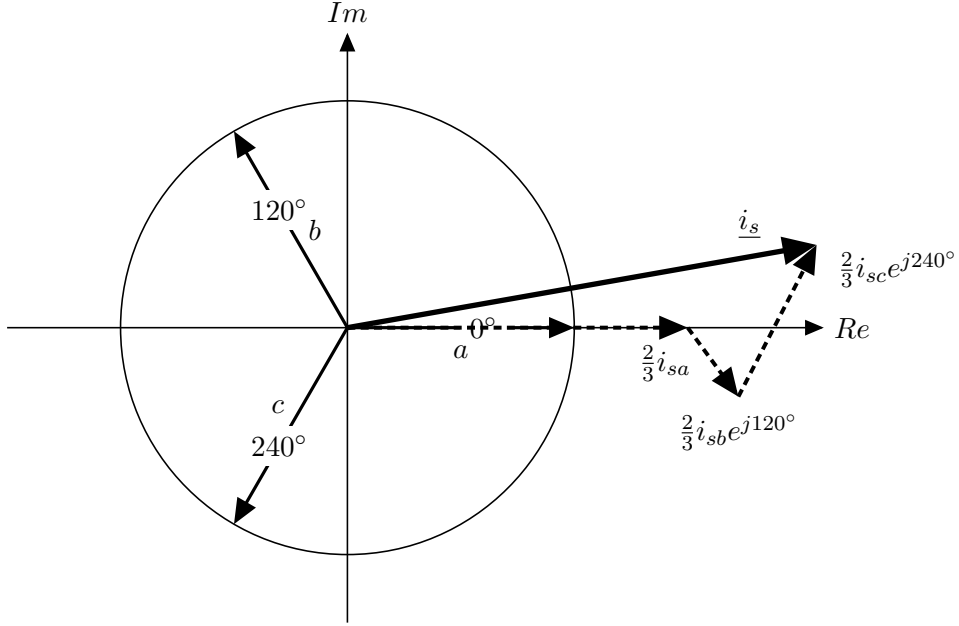


Figure 2.3: Stator current vector from three phase quantities.

The projected vector i_s represent the phase currents on the winding axes, in the same way it is possible to represent the three phase quantities of stator and rotor voltage and stator and rotor flux as the complex vectors \underline{u}_s , \underline{u}_r and $\underline{\Psi}_s$, $\underline{\Psi}_r$, respectively. These vectors all rotate with the stator frequency f_s . By implementing a Cartesian coordinate system which rotates with this angular speed it is possible to express the complex vectors for current, stator and rotor voltages and stator and rotor flux in the two components direct, d , and quadrature, q , as shown in equations (2.14) to (2.16)

$$\underline{i}_s = i_{sd} + j i_{sq}; \underline{i}_r = i_{rd} + j i_{rq} \quad (2.14)$$

$$\underline{u}_s = u_{sd} + j u_{sq}; \underline{u}_r = u_{rd} + j u_{rq} \quad (2.15)$$

$$\underline{\Psi}_s = \Psi_{sd} + j \Psi_{sq}; \underline{\Psi}_r = \Psi_{rd} + j \Psi_{rq} \quad (2.16)$$

If the real axis d is chosen identical with the direction of the permanent magnet flux linkage, Ψ_m , the q -component of the flux will be zero for the PMSM specific case. From this view it is possible to create an expression for electromechanical torque using the Ψ_m and the q -component of the stator current,

$$\tau_{em} = \frac{3}{2} i_{sq} \Psi_m \cdot n_p \quad (2.17)$$

where τ_{em} is the electromechanical torque, i_{sq} the q component of the stator current, Ψ_m the permanent magnet flux linkage and n_p the number of pole pairs.

The d-component of the stator current, i_{sd} is aligned to the rotor flux, Ψ_{rd} , and thus kept constant at zero unless field weakening is used. This in turn allows the cross-component of the current, i_{sq} , to control the torque, τ_{em} .

The dq-system explained above is a field-synchronous coordinate system that is aligned with the rotor flux. What this means is that the coordinate system is fixed to a rotating reference frame, whose rotation is synchronous to the rotation of the rotor. It is, however, possible to express these quantities in a stator-fixed, stationary coordinate system. By selecting the d-axis to be identical with one of the three winding axis, e.g. the axis for phase a flux it will be stator fixed. This new system is called the $\alpha\beta$ -coordinate system. Its relation to the three-phase system is expressed as follows,

$$\begin{bmatrix} s_\alpha \\ s_\beta \end{bmatrix} = \frac{2}{3} \begin{bmatrix} 1 & -\frac{1}{2} & -\frac{1}{2} \\ 0 & \frac{\sqrt{3}}{2} & -\frac{\sqrt{3}}{2} \end{bmatrix} \begin{bmatrix} s_a \\ s_b \\ s_c \end{bmatrix} \quad (2.18)$$

$$\begin{bmatrix} s_a \\ s_b \\ s_c \end{bmatrix} = \frac{2}{3} \begin{bmatrix} 1 & 0 \\ -\frac{1}{2} & \frac{\sqrt{3}}{2} \\ -\frac{1}{2} & -\frac{\sqrt{3}}{2} \end{bmatrix} \begin{bmatrix} s_\alpha \\ s_\beta \end{bmatrix} \quad (2.19)$$

and between $\alpha\beta$ and dq ,

$$\begin{bmatrix} s_\alpha \\ s_\beta \end{bmatrix} = \begin{bmatrix} \cos(\theta) & -\sin(\theta) \\ \sin(\theta) & \cos(\theta) \end{bmatrix} \begin{bmatrix} s_d \\ s_q \end{bmatrix} \quad (2.20)$$

$$\begin{bmatrix} s_d \\ s_q \end{bmatrix} = \begin{bmatrix} \cos(\theta) & \sin(\theta) \\ -\sin(\theta) & \cos(\theta) \end{bmatrix} \begin{bmatrix} s_\alpha \\ s_\beta \end{bmatrix} \quad (2.21)$$

where s is an arbitrary vector component and θ is the transformation angle,

$$\theta = \int_0^t \omega_r dt \quad (2.22)$$

The equations below show the current vector \underline{i}_s represented in the three coordinate systems,

$$\begin{aligned}
\underline{i}_s &= \frac{2}{3}(i_{sa}(t) + i_{sb}(t)e^{j\gamma} + i_{sc}(t)e^{2j\gamma}) \\
\underline{i}_s^s &= i_{s\alpha} + j i_{s\beta} \\
\underline{i}_s^r &= i_{sd} + j i_{sq}
\end{aligned} \tag{2.23}$$

where the indices s and r stands for stator and rotor fixed [9].

2.2 Converter

If the operation of a PMSM is to be controlled and not simply synchronised to the grid it has to be connected through a converter. This section will go through different ways in which converter faults can occur and the different topologies in which a three-phase converter can be configured.

2.2.1 Faults in Converter

For three phase converters, faults often appears due to failure of semiconductor devices. These faults may result in system shutdown with severe consequences depending on the application. Continuously operation is of great importance in both the automotive and power generation industries as stated previously.

A fault at one of the three different phase legs is manageable, as the two remaining phases can produce the rotating magnetic field needed to operate the machine. Faults including more than one converter leg will not be considered, as it is impossible to achieve a rotating field from only one healthy phase.

Faults at one of the phases in a three phase converter are mainly of four different types. Firstly, open circuit phase faults, with either one or both transistors out of order. Secondly, short circuit phase faults, with either one or both transistors out of order. Short circuit faults with both transistors needs a rapid shut down of the system, in order to prevent damage of the system [10].

In the case with a healthy, symmetrical system, the currents at any given time will sum up to zero as seen in (2.12). However, when one of the phases is disconnected, for example $i_c = 0$, during a fault in the converter, the system will be unbalanced. The simplest way of rebalancing the system would be to set $i_a = -i_b$ but this would not be able to operate the machine, as the magnetic field would not be rotating but simply pulsating back and forth. By connecting the wye-point of the machine to converter

the asymmetrical current i_0 will be introduced and the now unbalanced (2.12) can be rewritten into,

$$i_0 = -i_a - i_b \quad (2.24)$$

2.2.2 Converter Topologies

From Section 2.2.1, when a phase fault occurs, the remaining two phases has to be switched separately to create a rotating field. This is done theoretically by the introduction of i_0 , from (2.24). For a practical implementation, this can not be done with a three legged converter. To manage this situation, a converter with a fourth connection to the wye-point of the machine is needed. Two different topologies are identified to fulfil this requirement and can be seen in Figure 2.4. The first option is a converter with an extra, fourth leg, controlling the current from the wye-point. The other option is a converter where it is possible to connect the wye-point to the middle of the DC-link, via a switch that is turned on when the fault is detected.

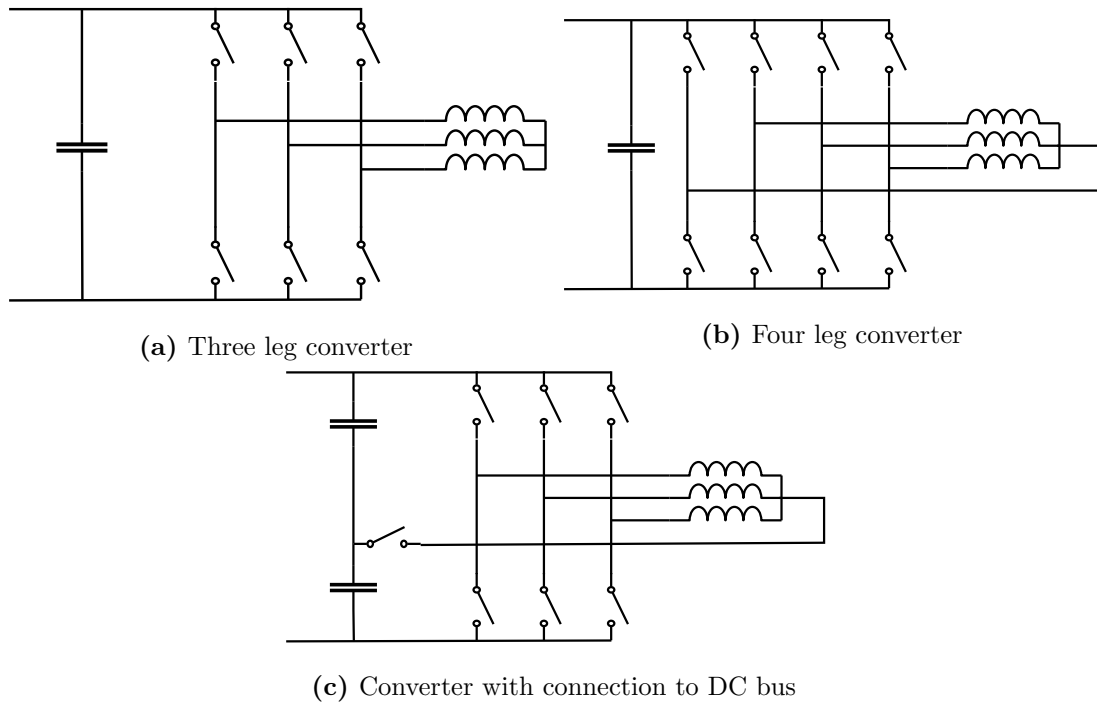


Figure 2.4: Converter topologies

2.3 Controller

In order to control the machine, the converter has to be switched in an appropriate way. This is done using a controller, that provides switching patterns to the converter. A common way of controlling a PMSM is FOC, field oriented control.

In this Section, the current controller will be built up from the electrical equations of the machine. The idea of FOC is to represent the three phase machine with two orthogonal vectors, and use a coordinate system that rotates with the rotor, as explained in Section 2.1.1. With this approach, the machine can be controlled in a similar way to a direct current, DC machine [10].

2.3.1 PI-controller

As shown in Section 2.1 a surface mounted PMSM can be treated as non-salient with the d- and q-components of the inductance being identical. Also, perfect field orientation is assumed, which gives that the torque only depends on the q-current (2.17).

Similar to the electrical equation for one phase of the machine, (2.2), the entire machine model can be expressed in vector form,

$$\underline{u}_s^s = R_s \dot{i}_s^s + \frac{d\Psi_s}{dt} \quad (2.25)$$

Where $\underline{\Psi}_s$ is the total flux. With $\frac{d\Psi_s}{dt}$ evaluated for a PMSM, the voltage equation is,

$$\underline{u}_s = R_s \dot{i}_s + L_s \frac{d\dot{i}_s}{dt} + j\omega_r L_s \dot{i}_s + j\omega_r \Psi_m \quad (2.26)$$

which describes the electrical properties of the machine, and will serve as a foundation of a controller block system. In (2.26), Ψ_m is the flux linkage from the permanent magnets, giving that $j\omega_r \Psi_m$ is the back-EMF of the machine. The term $j\omega_r L_s \dot{i}_s$ is the cross coupling between the d and q currents in the model, which appears due to the transformation in to the dq-frame. Replacing the back-EMF with \underline{E} and applying the Laplace transformation on (2.26) gives, after rearrangement,

$$\dot{i}_s = \frac{1}{sL_s + R_s + j\omega_r L_s} (\underline{u}_s - \underline{E}) \quad (2.27)$$

which is realised in Figure 2.5. This equation describes the output \dot{i}_s as a function of the voltage fed to the machine, the rotational speed and machine constants. \underline{u}_s is the voltage applied on the machine, which is what will be controlled with respect to the characteristics of the machine.

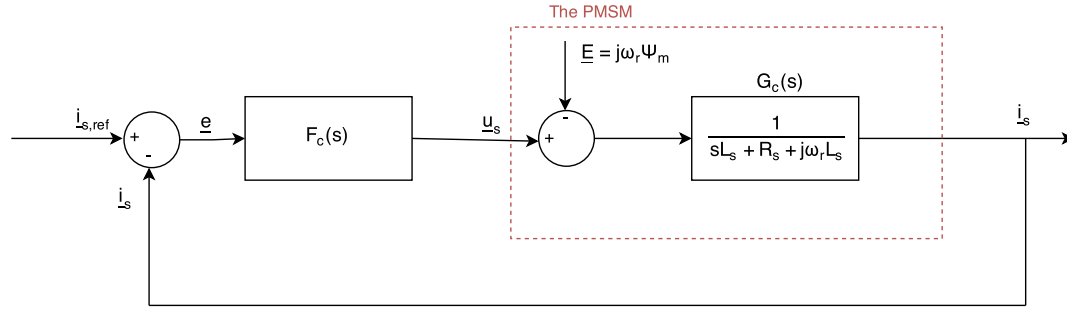


Figure 2.5: Machine and controller block system

Firstly, to compensate for the back-EMF \underline{E} , in (2.27), a feed forward of back emf, $\hat{\underline{E}} = j\omega_r \hat{\Psi}_m$ is added, where $\hat{\cdot}$ denotes the value to be estimated.

Secondly, the cross-coupling inductance in the machine has to be decoupled, this is accounted for by implementing a feed forward loop with the multiplying factor $j\omega_r \hat{L}_s$. To increase the error tolerance active damping, also called active resistance, R_a is added in the same feed forward loop. This will dampen the response to large error terms by subtracting $\underline{i}_s R_a$ from the input \underline{u}_s .

This results in a new voltage reference to the machine,

$$\underline{u}_s = \underline{u}'_s + (j\omega_r \hat{L}_s - R_a) \underline{i}_s + \hat{\underline{E}} \quad (2.28)$$

where the $'$ denotes the term \underline{u}'_s to be the uncorrected value of \underline{u}_s before adding the feed forward terms. This new compensated current regulator is shown in Figure 2.6.

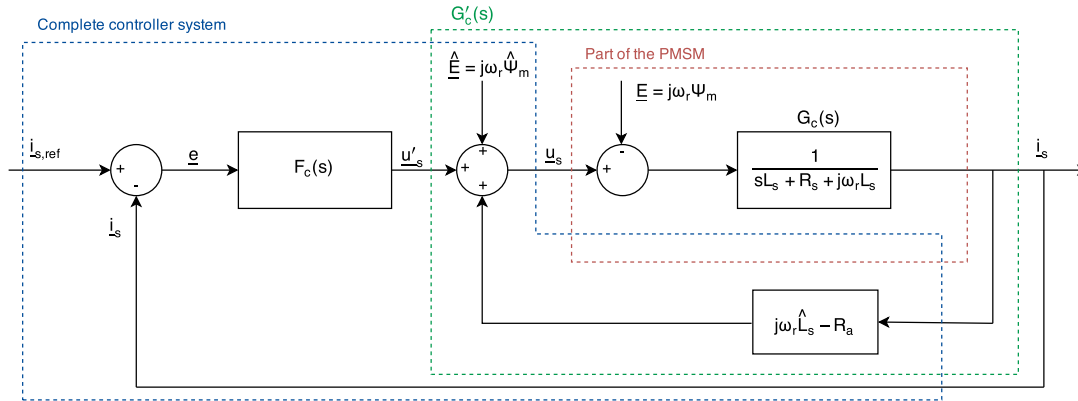


Figure 2.6: Current regulator design

To derive the the controller, a new closed loop system is derived, including the new voltage reference from the controller.

When the voltage reference from (2.28) is set as equal to the machine voltage from (2.26), the following is obtained after Laplace transformation,

$$R_s \dot{i}_s + sL_s \dot{i}_s + j\omega_r L_s \dot{i}_s + j\omega_r \Psi_m = \underline{u}'_s + (j\omega_r \hat{L}_s - R_a) \dot{i}_s + \hat{E} \quad (2.29)$$

by assuming perfect estimations, the equation is reduced to,

$$R_s \dot{i}_s + sL_s \dot{i}_s = \underline{u}'_s - R_a \dot{i}_s \quad (2.30)$$

which can be rewritten as,

$$\frac{\dot{i}_s}{\underline{u}'} = \frac{1}{sL_s + R_s + R_a} \quad (2.31)$$

this is realised in Figure 2.7.

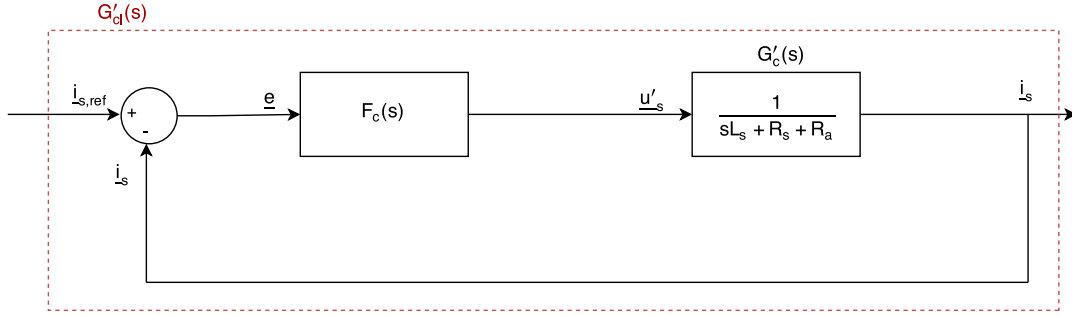


Figure 2.7: Closed loop system

To find the setting parameters of the controller, the closed loop system G_{cl} designed to be a first order low pass filter, giving it the transfer function,

$$G_{cl} = \frac{i_s}{i_{sref}} = \frac{\alpha_c}{s + \alpha_c} = \frac{\alpha_c/s}{1 + \alpha_c/s} = \frac{F_c(s)G'_c(s)}{1 + F_c(s)G'_c(s)} \quad (2.32)$$

where α_c is the bandwidth. By identification,

$$\frac{\alpha_c}{s} = F_c(s)G'_c(s) \Rightarrow F_c(s) = \frac{\alpha_c}{s} G_c'^{-1}(s) = \frac{\alpha_c}{s} (s\hat{L}_s + \hat{R}_s + R_a) \quad (2.33)$$

By rewriting (2.33) the proportional, K_{pc} , and integral, K_{ic} gain constants of the filter can be found,

$$F_c(s) = \alpha_c \hat{L}_s + \frac{\alpha_c(\hat{R}_s + R_a)}{s} = K_{pc} + \frac{K_{ic}}{s} \quad (2.34)$$

Identification from (2.34) gives that,

$$K_{pc} = \alpha_c \hat{L}_s \quad (2.35)$$

$$K_{ic} = \alpha_c(\hat{R}_s + R_a) \quad (2.36)$$

R_a can be determined by setting the bandwidth for the regulator, $F_c(s)$, to the same value as for the entire system, $G'_c(s)$,

$$G'_c(s) = \frac{1}{sL_s + R_s + R_a} = \frac{1/L_s}{s + (R_s + R_a)/L_s} = \frac{g\alpha_c}{s + \alpha_c} \quad (2.37)$$

with this approach, it can be seen that

$$\alpha_c = \frac{\hat{R}_s + R_a}{\hat{L}_s} \Rightarrow R_a = \alpha_c \hat{L}_s - \hat{R}_s \quad (2.38)$$

2.3.2 Resonant controller

A PI controller is capable of handling DC quantities, which makes it ideal for for controlling a symmetrical three phase machine, with quantities transformed into the rotating dq reference frame [11]. However, when a phase fault occurs, the system is no longer symmetrical, and the PI-controller is no longer capable of delivering a stable torque. The two remaining phases will still be able to create a rotating magnetic field and thus operate the machine, but the torque will be oscillating with a frequency of two times the electrical speed. This is due to the phase shift in the unbalanced system. In the balanced, three phase system, the currents are shifted with 120° , creating a symmetrical system. When one phase is broken, the two remaining phases will compensate by moving 30° towards each other, due to the dq0 transformation.

Existing research suggest an additional part, a resonant controller to be added in parallel to the PI controller, in order to reject the sinusoidal function of 2θ , which is caused by the unbalanced system, and the phase shifts. In Figure 2.8, the control system with the proposed resonant control part is shown [11, 12].

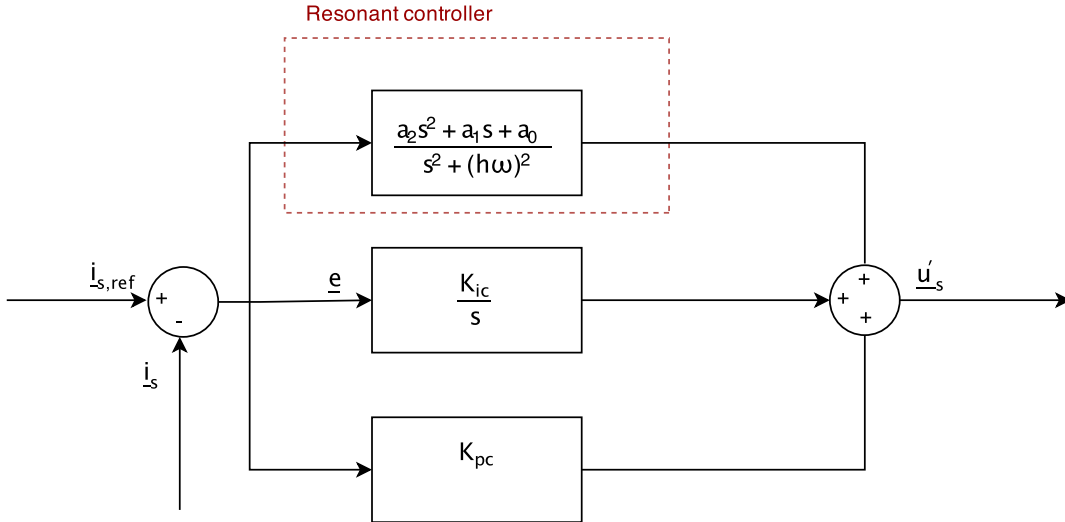


Figure 2.8: Controller with resonant part

To keep the fast performance of the PI controller at low frequencies, a_0 is chosen to be zero [11]. Furthermore, to simplify the tuning of the system, a_2 is chosen to be zero as well. As the objective is to counteract the second harmonic in the system, $h = 2$, and ω is the electrical rotor speed. a_1 is set to be high, to get as close as possible to an infinite gain, and in that way, eliminate the oscillations in the torque.

2.4 Pulse width modulation

To switch the converter according to the voltage reference from the controller, the signal can not be delivered as an analog reference. Therefore, pulse width modulation, PWM, is needed before sending the switching pattern to the converter. In order to create the PWM signals, the voltage reference has to be recalculated in relation to U_{DC} giving a relative reference between 0 – 1,

$$SR = 0.5 + 0.5 \frac{2}{U_{DC} U_{a,ref}} \quad (2.39)$$

where SR is the switch ratio.

3

Lab setup

This chapter contains methodology, equipment choice and calibration for both the machine characterisation and the tests performed.

The main test object was the NewGen PMSM described in Appendix A.1. The machine was however connected to a drive train consisting of an induction machine and a gear box at all times. Due to this the parameters acquired in the characterisation, more specifically the mechanical parameters inertia, J , damping constant, b and Coulomb friction, J_0 , are those of the entire system, as seen in Figure 3.1.

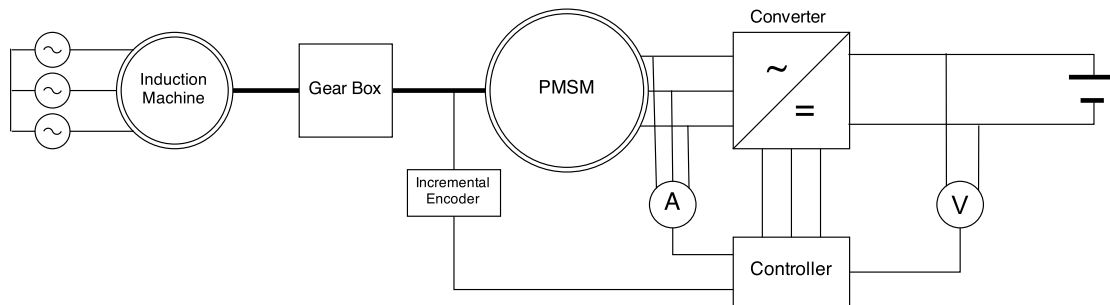


Figure 3.1: Lab setup

When in generator operation the PMSM was driven by the induction machine, presented in A.2, which was fed by a converter. When used as a motor the converter was fed by a DC machine. The gearbox was needed to match the relatively high speed induction machine, $\Omega_n = 1540$ rpm, to the slow PMSM, $\Omega_n = 100$ rpm.

The main part of the setup, from the grid connection of the induction machine to the PMSM was fixed and not changed for this project. There was however still the task of choosing and calibrating the position sensor, converter and control system.

3.1 NewGen

The NewGen is a prototype PMSM intended for direct drive in large wind turbines. It uses a rotor which is located outside of the stator creating a better load path. Furthermore, it has the bearings placed adjacent to the air-gap. These features are intended to lessen the rigidity requirements for both the rotor and the stator leading to large mass reduction in the mechanical structure allowing larger a diameter. The bearings used will also be a lot smaller compared with the ones placed around a large central axis making repairs easier and more accessible. The increased diameter means a mass reduction of the electrical components resulting in machines with larger diameter and lower weight than would have been otherwise possible [13].

The technical data and machine specification are presented in A.1.

3.2 Controller

The hardware for the control of the converter is dSPACE 1103, which consists of a real time processor and comprehensive I/O board. The controller board is shown in Figure 3.2. The controller board includes four analog input ports with one AD converter each, and 16 analog input ports sharing a total of four AD converters. Furthermore, there are seven input ports for incremental encoders, and PWM output ports available.

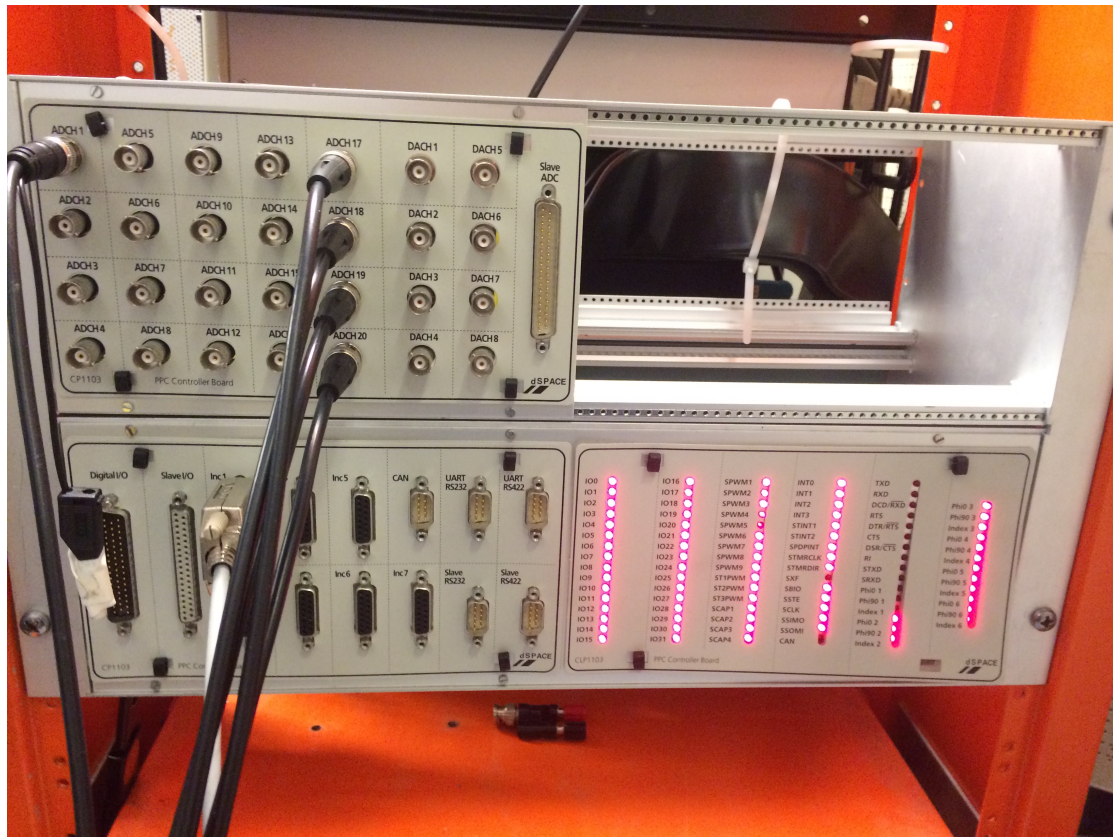


Figure 3.2: dSPACE Hardware

The controller is possible to implement in two different ways, as C-code, using predefined routines for the dSPACE 1103 processor, or by building the controller in Simulink and run it with a Real Time Interface, which is an interface which provides Simulink and dSPACE to fully interact with each other.

Using Simulink Real Time Interface, the controller is modelled using both Simulink standard library and the additional RTI library, which enables control of the I/O interface. RTI includes functions for creating PWM signals, as well as reading data from the encoder and the AD converters.

3.2.1 Real time interface

Simulink RTI is a real time interface in Simulink, which enables interaction with dSPACE, and to create real time code executed in the dSPACE 1103 CPU. Additionally to the Simulink block set, dSPACE offers a couple of more block sets, in order to interact with the DSP in the dSPACE environment.

In this setup, in addition to regular Simulink blocksets, blocks for PWM generation, blocks for enable reading from the inputs to dSPACE, and blocks with pre defined functions for reading the signals from the encoder has been used.

ControlDesk 3.7.1 is the RTI software used to control parameters to the controller and observe the system during the tests and also to capture variables for further evaluation in MATLAB. ControlDesk is provided from dSPACE, and interacts with the controller generated from Simulink. For example, all parameters in the Simulink controller model can be watched in ControlDesk, and constants in the model can be changed during the test. An overview of ControlDesk is given in Figure 3.3.

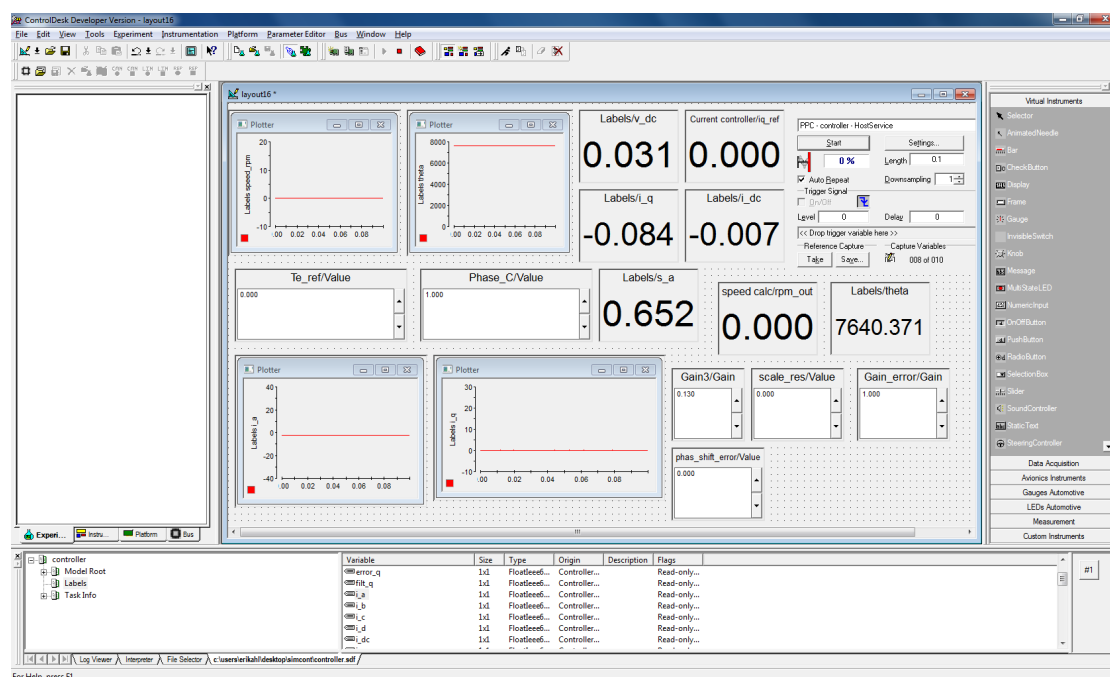


Figure 3.3: dSPACE Software

The PWM three phase generation block is from Simulink RTI, and generates PWM signals for the interface out port, later connected to the converter. The dead band time for the PWM generation needs to be put between 0 and 100μ . To determine a appropriate value, the characteristics of the IGBT's has to be studied. From [14], it is clear, that a dead band of $1\mu s$ is long enough to cover the turn off of one IGBT, as the turn of delay time is $460ns$, and the fall time is $30ns$.

3.3 Position sensor

In order to set up the controller in Section 2.3, it is vital to know the speed and position of the rotor. The need of this information requires a position sensor, and there

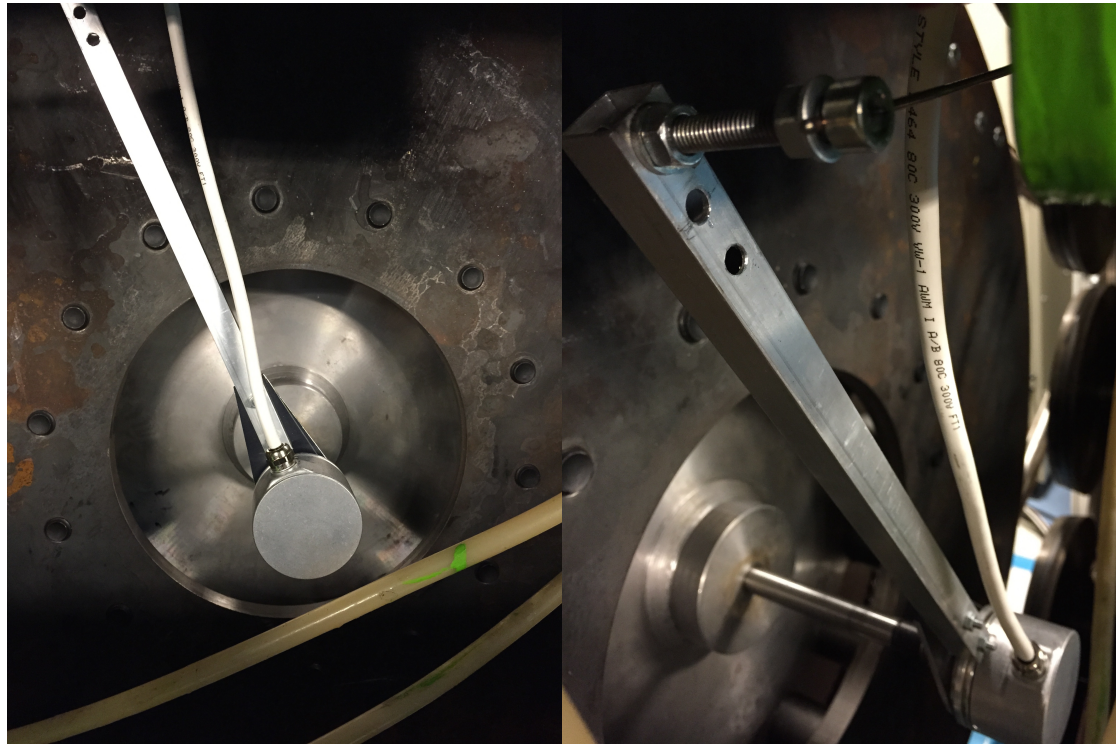
are different types available. From the Hardware Installation and Configuration manual of the dSPACE RTI system, [15], dSPACE 1103 is prepared with an interface for incremental encoders. Incremental encoders typically have two outputs, all of them with square waves. The two pulses, often A and B , are 180 degrees long and 90 degrees internally shifted. Due to the two pulses and the shift, the encoder is able to operate in different directions. A third signal, Z is often added, and it gives one pulse per mechanical revolution, which is used as a reset signal. This makes it possible to reset the position.

In order to get good resolution from the encoder, it needs to give a certain number of pulses per electrical period. From A1, we have 16 pole pairs in our PMSM, which implies that we have 5760 electrical degrees each mechanical revolution.

For a controller switching at $10kHz$ the resolution had to be around three degrees per pulse from the encoder, for a machine rotating at 100 rpm with 16 pole pairs. From the supplier, only encoders with 1024 or 5000 pulses per revolution were available and the one with 1024 was considered to have too low resolution. Therefore, an encoder with 5000 pulses per revolution was chosen, the Hengstler Rotary incremental encoder 5000, RI58-O/5000AS.41RB, A.6.1.

3.3.1 Encoder instalment and calibration

The chosen encoder was installed on the PMSM by an outside party. Due to an error in the machine design, the axle to which the encoder was connected was not fully centred. By mounting the encoder on a swing arm, see Figure 3.4, allowing it to rotate with the secondary rotation of the axle, the position could still be measured.



(a) Mounting of the encoder.

(b) Encoder swing arm.

Figure 3.4: Solution to the secondary rotation of the incremental encoder mounting axle.

This did however cause problems with the position output. The tension of the swing arm and the rotation of the mounting axle meant the encoder itself accelerated with the rotation of the machine two times per revolution and decelerated twice. This resulted in wave shape of the position output and the speed calculated thereof, even though the real speed of the machine was constant. By extrapolating the ideal position output and calculating the difference from what the encoder gave it was possible to observe the behaviour of the offset, this is shown in Figure 3.5.

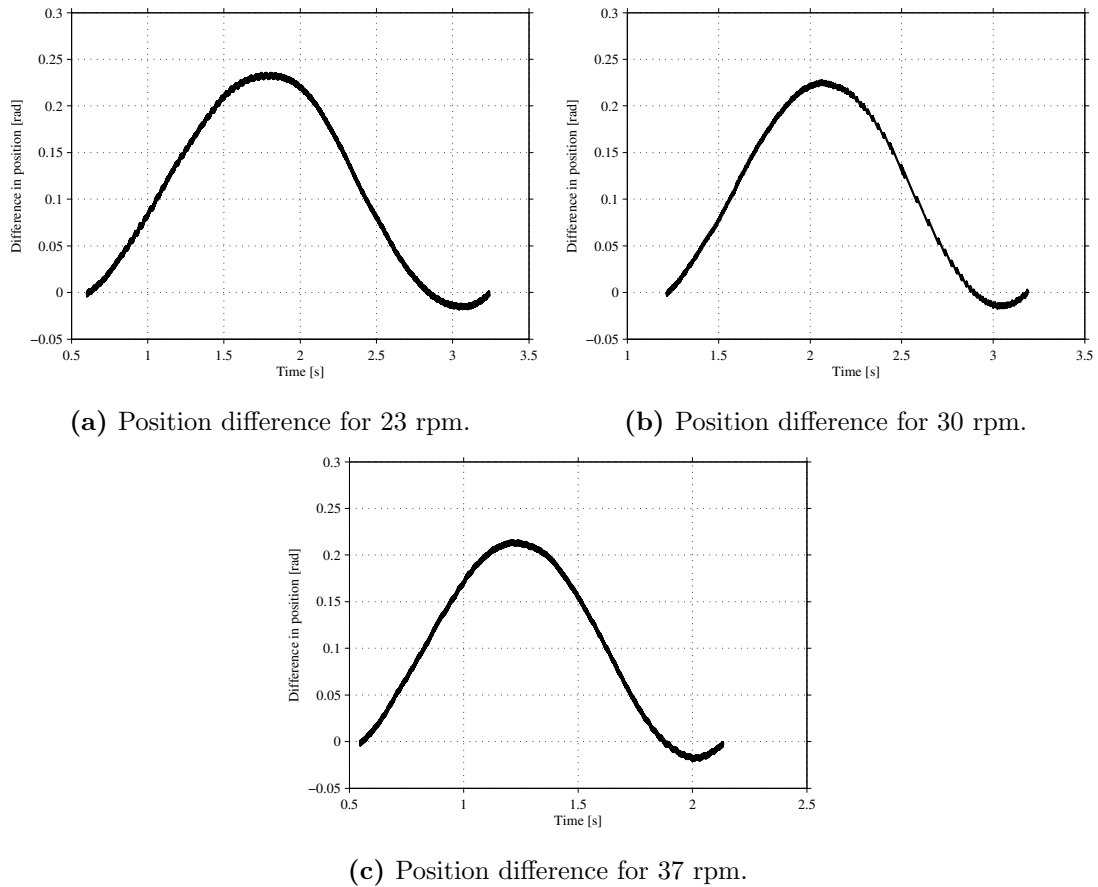


Figure 3.5: Difference in position measurement from ideal conditions [mechanical rad].

The difference seen is over one mechanical revolution. The results are very similar and shows a clear sinusoidal shape, shifted forward and with an average above zero. A few simple calculations showed that the average horizontal offset was 2.405 rad and the vertical offset was 0.13 rad.

3.4 Converter

The converter used to run the machine has a four leg topology. It is built with IGBT's of the type Semikron SKM 300 GB 125D as transistors. The converter in the lab is normally built to be working as a four leg converter, as presented in Section 2.2.2, making it possible to introduce open circuit phase faults. However, in the actual converter, one phase is broken, giving slightly less options when introducing the open phase fault.

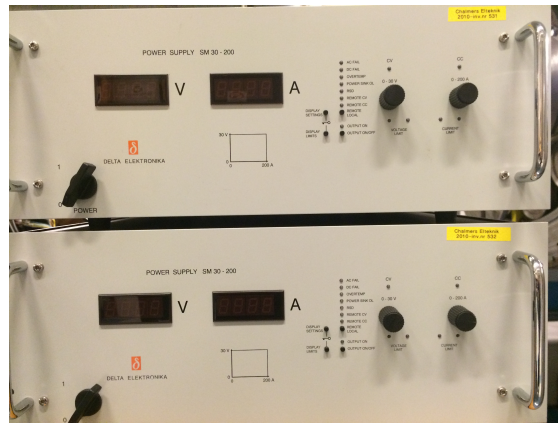
3.5 Current measurement

Built in the converter, there are LEM modules for current measurement, of the type LEM. The output from the LEM's are a voltage between 0-10 V for a current range of 0-300 A.

3.6 DC Power Supply

DC power is available in two different ways in the lab. Regulated DC power supply boxes from Delta Elektronika shown in Figure 3.6a, from the product range SM 6000. In the lab, two boxes were available of the type SM 30-200, each producing 30V, 200A, with a total of 6000W each. When connected in series, they can supply the converter with 60V, 200A and a total of 12000W.

The other voltage source is accessed from a power outlet in the wall in the lab. This power comes from a DC machine in the building, and it can produce a higher voltage than the boxes from Delta Elektronika. The DC source can be regulated all the way up to 800V, which is more than enough to run the NewGen machine at rated speed. The maximal current aloud in the converter is limited to 100 A. This voltage source is regulated with a box from ABB, seen in Figure 3.6.



(a) DC power supply boxes



(b) Regulator box for DC source

Figure 3.6: Regulation of the two different DC sources.

4

Machine Characterization

In order to create accurate simulations and furthermore successfully control the complete system the characteristics of said system had to be determined. There were however a few assumptions made.

In accordance with Section 2.1 a smooth air-gap model was used, which means the cogging torque between permanent magnet and stator teeth was neglected. Inductance was assumed to be position independent and magnetic saturation was neglected. In the electrical conduction loss model both core losses in the magnetic materials and the frequency dependence of the stator resistance were neglected.

4.1 Tests

The parameters in need of determination in order to create a satisfactory representation of the machine are presented Table 4.1.

Table 4.1: Parameters for simulation application

	Parameter
Stator resistance	R_s
Stator inductance	L_s
Mutual inductance	M
Permanent magnet flux linkage	Ψ_m
Inertia	J
Damping constant	b
Coulomb friction	J_0
Number of pole pairs	n_p

Stator resistance, inductance and the mutual inductance are needed for the electrical model of the machine as seen in Equation (2.11). Inertia, damping constant and coulomb friction are needed for the mechanical model, described in equation (2.1). The permanent magnet flux linkage is needed for (2.17), used in the electrical model and the number of pole pairs determine the relation between the mechanical and electrical speed of the machine.

4.1.1 Stator resistance and inductance

To acquire the stator resistance and inductance for the PMSM an AC standstill test was performed. However, it was not a locked rotor test, as only the inertia kept the machine at the same place. Figure 4.1 shows the connections on a circuit representation of the machine.

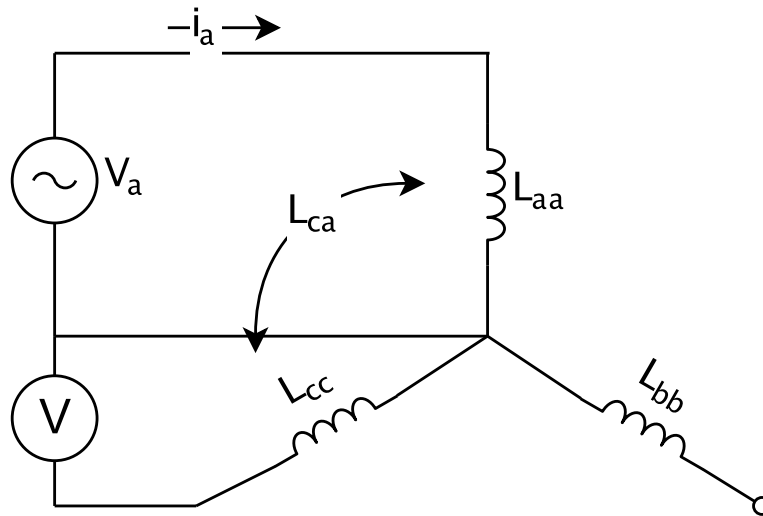


Figure 4.1: AC standstill test connection.

By applying a voltage to one phase at the time and measuring the current through and the voltage over the phase it was possible to gain phase shift between voltage and current. Thereby being able to calculate the stator resistance and self inductance of that particular phase,

$$\frac{U \angle 0}{I \angle -\phi} = Z \angle \phi = R + j\omega L \quad (4.1)$$

where U is the value of the voltage applied over the phase, I is the current, $-\phi$ is angle with which the current is shifted from the voltage, Z is the phase impedance later divided into R and L . L is the self and leakage inductance, but to be able to make a accurate representation the mutual inductance was also needed. By measuring the induced voltage this was calculated in accordance with,

$$M = \frac{U_{ind}}{\omega I_{main}} \quad (4.2)$$

where M is the mutual inductance, U_{ind} the induced voltage and I_{main} the current in the connected phase.

The test was performed for two different rotor positions to investigate the position dependance of the inductance and for two different current levels through the main winding. In order to control the amount of current being drawn and being able to apply the right voltage two transformers were used. One variable transformer and a 1:10.25 fixed transformer with delta-wye connection to transform the current to 50 A and 130 A respectively. The system was connected to the 50 Hz grid.

4.1.2 Flux linkage evaluation

In a PMSM, the magnetic field is created by permanent magnets placed in the rotor along with the stator currents. When working as a generator, the machine is mechanically driven by an external source and the rotating rotor will induce a voltage in the stator, the back-EMF. Back-EMF is proportional to the angular speed of the rotor, which implies that if the induced voltage and the speed is known, the magnetic flux constant can be determined, as explained in Section 2.1 and (2.4). The peak-to-peak back-EMF was measured between phase and neutral when the machine was in open circuit and rotated. This was performed for all three phases.

The external source used to drive the PMSM as a generator was the induction machine shown in Chapter 3. The back-emf measurements were taken at three different speeds at steady state conditions.

4.1.3 Machine damping

For this test the machine was driven as a torque controlled motor. In the mathematical machine model, (2.1), two constants are needed, the damping constant, b and Coulomb friction, J_0 .

In steady state and no load the following apply,

$$\begin{aligned}\frac{d\omega_r}{dt} &= 0 \\ \tau_L &= 0\end{aligned}\tag{4.3}$$

From (2.1) it can then be derived,

$$\tau_{em} = b\omega_r + J_0\tag{4.4}$$

where τ_{em} is given by (2.17). Thus, by taking measurements at six steady state speeds and creating a linear fit approximate values for b and J_0 were acquired.

4.1.4 Inertia

To determine the inertia of the system the mechanical model in (2.1) was used once more. The test used (also known as a coast down test) meant driving the machine as a motor

and suddenly stop switching the converter while measuring the coast down behaviour, which was done for three different initial speeds, ω_{r0} . When the machine is allowed to slow to a halt in this way $\tau_{em} = \tau_L = 0$. Thus, from (2.1), the mechanical speed,

$$\omega_r = \left(\omega_{r0} + \frac{J_0}{b} \right) e^{-\frac{b}{J}t} - \frac{J_0}{b} \quad (4.5)$$

By creating an exponential curve fit using the normalized root mean square deviation method in MatLab values for the inertia, J , was acquired.

4.2 Results and analysis

In this section the results using the methods described in section 4.1 is presented.

4.2.1 Resistance and inductance measurements

Figure 4.2 shows the main voltage, phase A, and induced voltage in phase B for 50 and 130 A for the two tested positions. The results were very similar for the other cases. As can be seen in Figure 4.2a and 4.2c there is comparatively more noise present for 50 A.

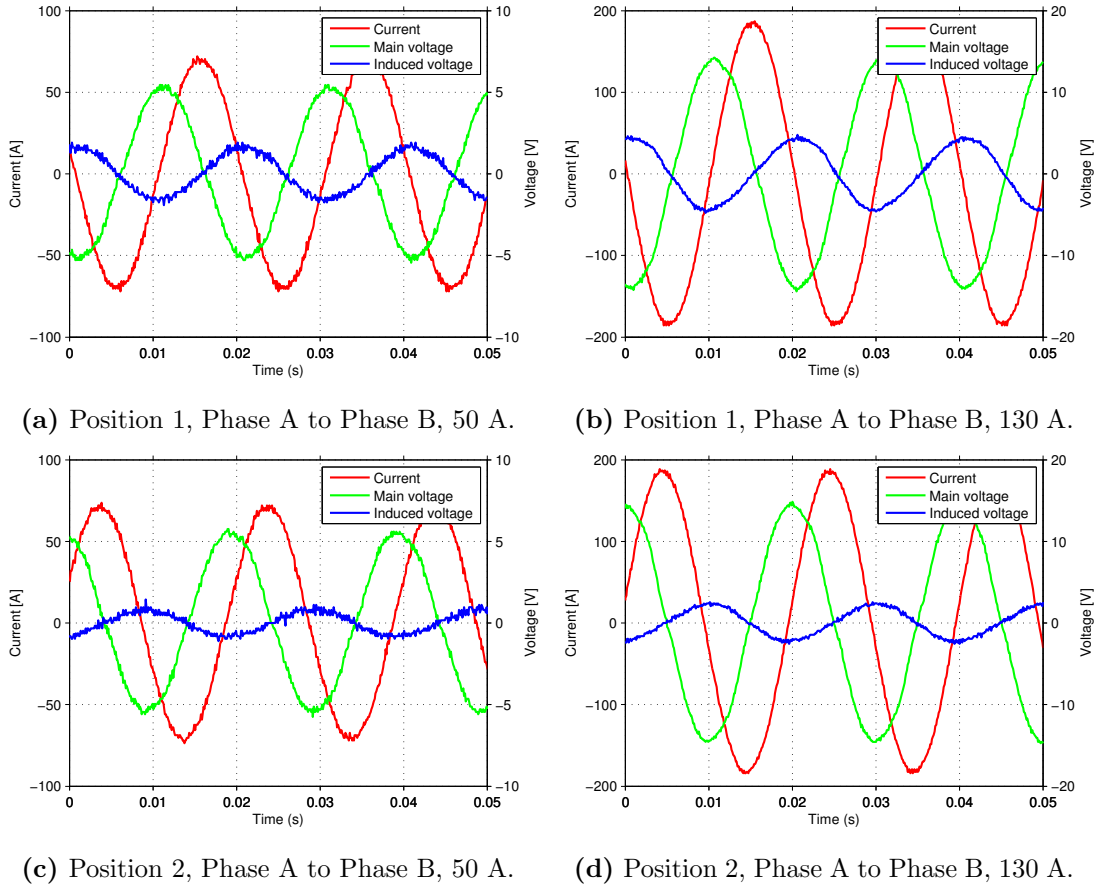


Figure 4.2: Main and induced voltages for two different positions and two current levels.

In Figure 4.3 the induced voltages for 130 A in all the phases can be seen. The phase shift between the voltages are simply due to the timing of the measurements. The amplitude difference however suggests a position dependence of the mutual inductance. Even though only the results from the 130 A tests are shown graphically all results were used for the calculations of resistance and inductance.

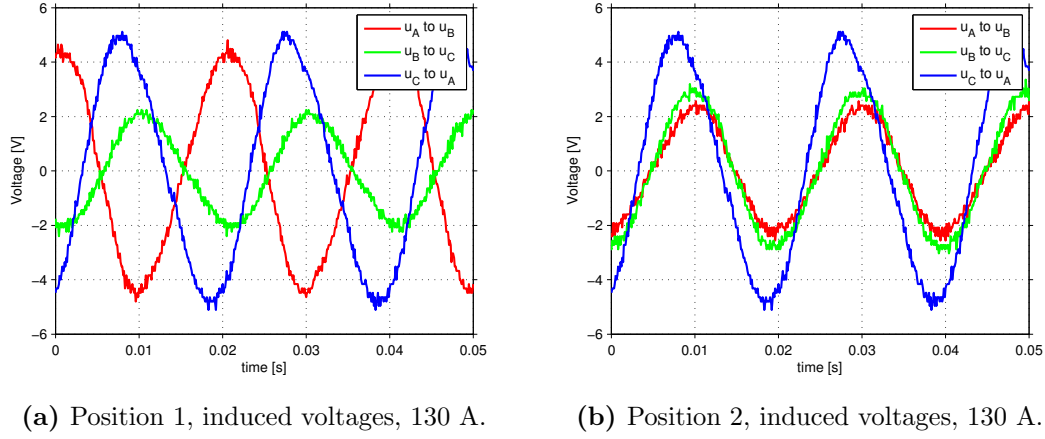


Figure 4.3: All induced voltages for the two positions.

The calculated values for stator resistance, stator inductance and mutual inductance for all tests are presented in Table 4.2.

Table 4.2: Stator resistance, all results in $m\Omega$.

	Resistance [$m\Omega$]		
	Phase A	Phase B	Phase C
Pos 1, 130 A	11.4	12.0	12.2
Pos 1, 50 A	12.3	13.0	13.2
Pos 2, 130 A	11.4	12.4	11.3
Pos 2, 50 A	12.6	13.7	12.5
	Inductance [μH]		
	Phase A	Phase B	Phase C
Pos 1, 130 A	241.7	254.7	258.4
Pos 1, 50 A	235.0	249.2	251.7
Pos 2, 130 A	249.6	271.6	247.8
Pos 2, 50 A	242.5	264.0	241.6
	Mutual inductance [μH]		
	Phase A to B	Phase B to C	Phase C to A
Pos 1, 130 A	76.46	35.61	67.85
Pos 1, 50 A	73.72	33.68	65.23
Pos 2, 130 A	38.78	49.77	83.86
Pos 2, 50 A	37.52	47.98	80.82

In Table 4.3 the average values are shown.

Table 4.3: Average values for stator resistance, inductance and mutual inductance.

	Resistance [$m\Omega$]	Inductance [μH]	Mutual inductance [μH]
Average value	12.3	250.6	57.61

4.2.2 Results from Ψ_m evaluation

Figure 4.4 the results from the back-emf measurements can be seen.

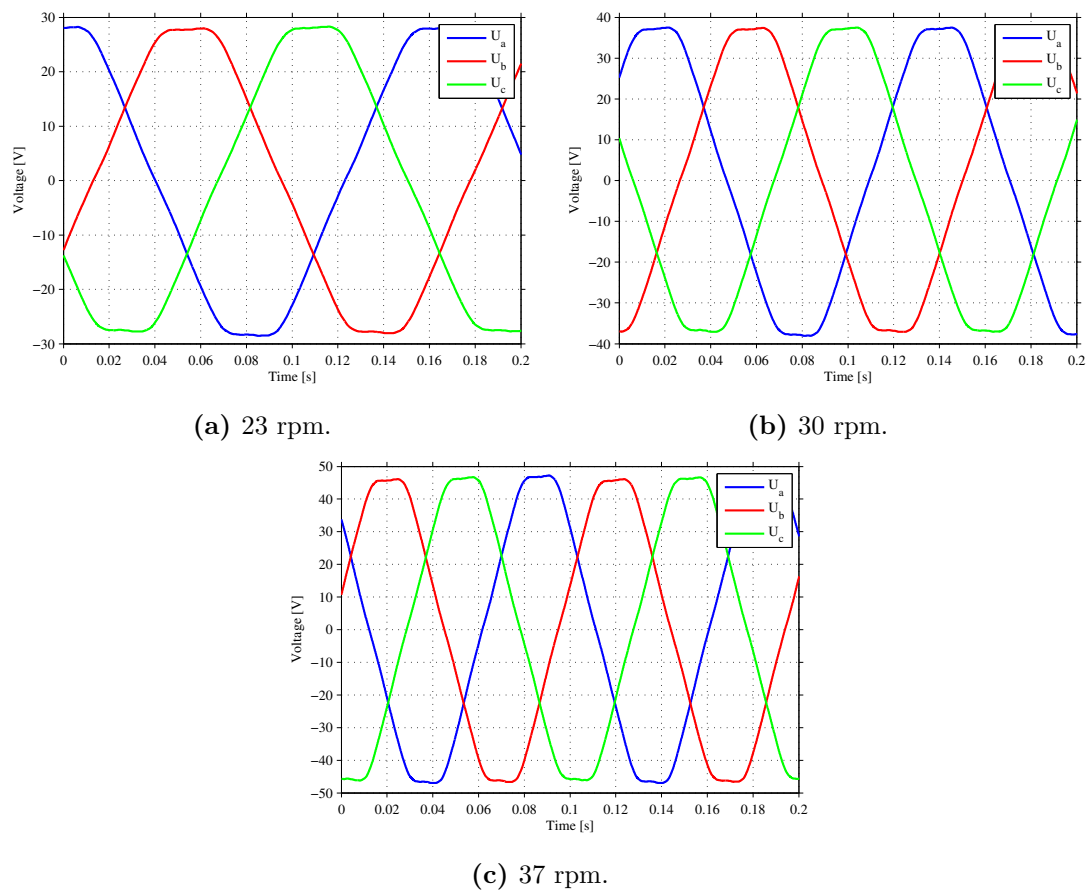


Figure 4.4: Measured back-emf for three different speeds.

In Table 4.4 the calculated back-emf constant Ψ_m for each rotation speed can be seen as well as the average value.

Table 4.4: Back-emf constant values.

	23 rpm	30 rpm	37 rpm	Average
Ψ_m	0.7339	0.7328	0.7309	0.7326

4.2.3 Machine damping results

Figure 4.5 shows terminal speed for different torque as well as linearised fits using different data points.

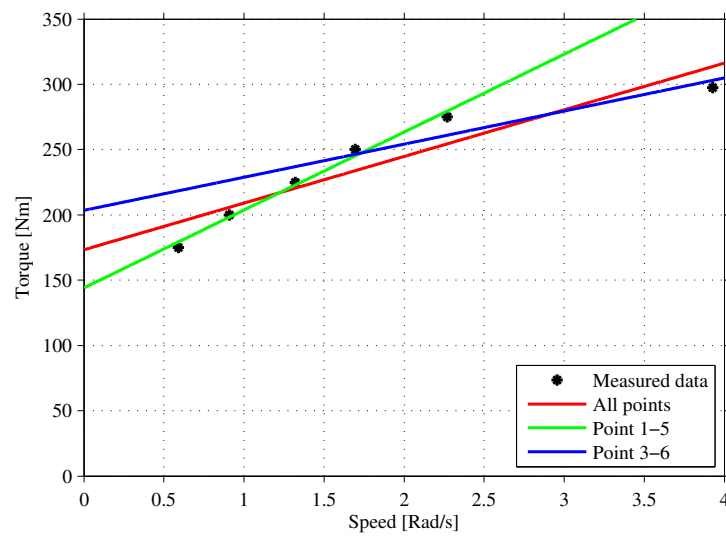


Figure 4.5: Torque-speed relation for tested operating points and linear curve fits for different data sets.

Table 4.5 shows the values of the machine damping constant, b , and Coulomb friction, J_0 gained from the curve fits, with the chosen values underlined.

Table 4.5: Machine damping constant, b , and Coulomb friction, J_0 .

Data points used	1-6	1-5	3-6
b	35.72	<u>59.67</u>	25.35
J_0	173.3	<u>144.0</u>	203.5

4.2.4 Results from Inertia test

In Figure 4.6 the results from the inertia test can be seen, the values from the curve fit including the average inertia are displayed in Table 4.6.

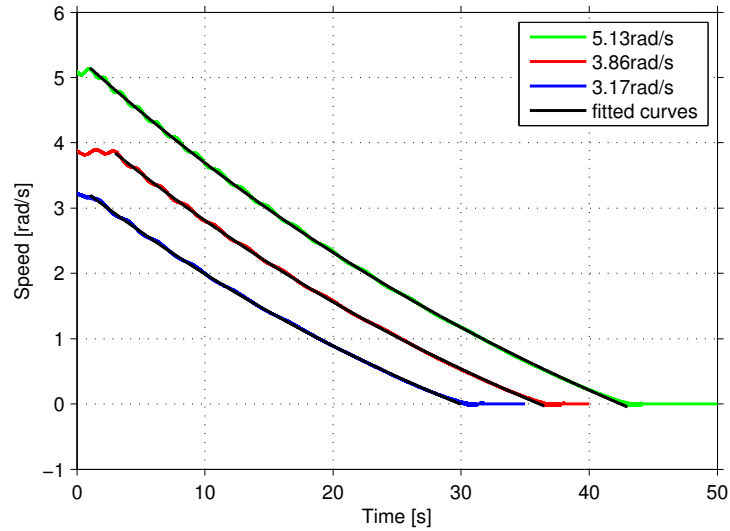


Figure 4.6: Coast down tests for three initial speeds and their fitted exponential curves.

Table 4.6: Machine inertia, J , for each initial speed and the average value.

	3.16 rad/s	3.86 rad/s	5.13 rad/s	Average
Inertia [kgm^2]	$2.820 \cdot 10^3$	$3.030 \cdot 10^3$	$3.324 \cdot 10^3$	$3.058 \cdot 10^3$

4.3 Discussion of results

Below a short discussion of the results from the machine characterisation is presented.

4.3.1 Stator resistance and inductance

As seen in Table 4.2 the calculated values for stator resistance and inductance are very similar for all tested cases. However, there seems to be a position dependent variance to the mutual inductance. This means the machine is not entirely non-salient as assumed. Even though the value of mutual inductance vary between $33.68 \mu H$ to $83.86 \mu H$ the difference is still small in relation to the main stator inductance which is why the average value is used even for the mutual inductance.

4.3.2 Flux linkage results

The results for the back-emf constant were very consistent for all tested speeds and thus speed invariant as was to be expected.

4.3.3 Machine damping equation

Figure 4.5 shows a clear outlier in the results for 300 Nm. When performing the test it was difficult to determine the terminal rotational speed for 300 Nm since the speed kept increasing very slowly with no indication to stop. The reason for this could be that the friction in the gearbox or the bearings decreased as the machine got warmer or that 300 Nm is enough to accelerate the machine to its maximum speed over time. This is however unclear which is why the results from measurement points 1-5 was chosen.

4.3.4 Inertia test

The acquired results are for the drive system as a whole, not just the test object PMSM, this is all in order since the system always moves as a whole. In Table 4.6 a slight speed dependence in the results can be detected, indicating that the model used might not be complex enough. However, the final inertia value used in the simulations was chosen using a start up comparison as well as the results from the inertia test.

5

System simulation

For the simulation of the electrical and mechanical behaviour, MATLAB and Simulink is used, and a complete model of the system is built up, using the results presented in chapter 4 4.

The model of the system was implemented in MATLAB and Simulink using both Simulink block sets and s-functions. An overview of the simulated system is given in Figure 5.1.

5.1 Model setup

The simulation model consists of the controller, built with the Simulink block set. The machine model, which is built in an s-file, utilised within an s-file block from the Simulink block set. Furthermore, a model over the mechanical behaviour of the system is implemented in an separate s-file as well. Moreover, in order to get a system that is easily used, a speed controller is used to set the speed in the simulations.

5.1.1 PMSM

The PMSM can be modelled in in stationary three phase reference frame or in the rotating dq0 reference frame. For the simulations in this thesis, the PMSM was implemented in the stationary three phase reference frame, which made it possible to run the machine with an open circuit fault, which is difficult to realise in a model made in the rotating dq0 reference frame, as the three phase currents were under observation. Furthermore, it is easy to implement the values from the machine characterisation in the stationary three phase reference frame, derived in Chapter 2.

The model of the PMSM is written in an external S-function, and connected to the Simulink interface in the block "S-function2", in Figure 5.1.

5.1.2 Controller

As the controller is built according to section 2.3.1, it is implemented in the rotating dq0 reference frame, implemented with Simulink block sets. It is built up inside the block "Controller" in Figure 5.1.

The current controller is modelled in Figure 5.2. The model implemented in Simulink is derived in Chapter 2.3.

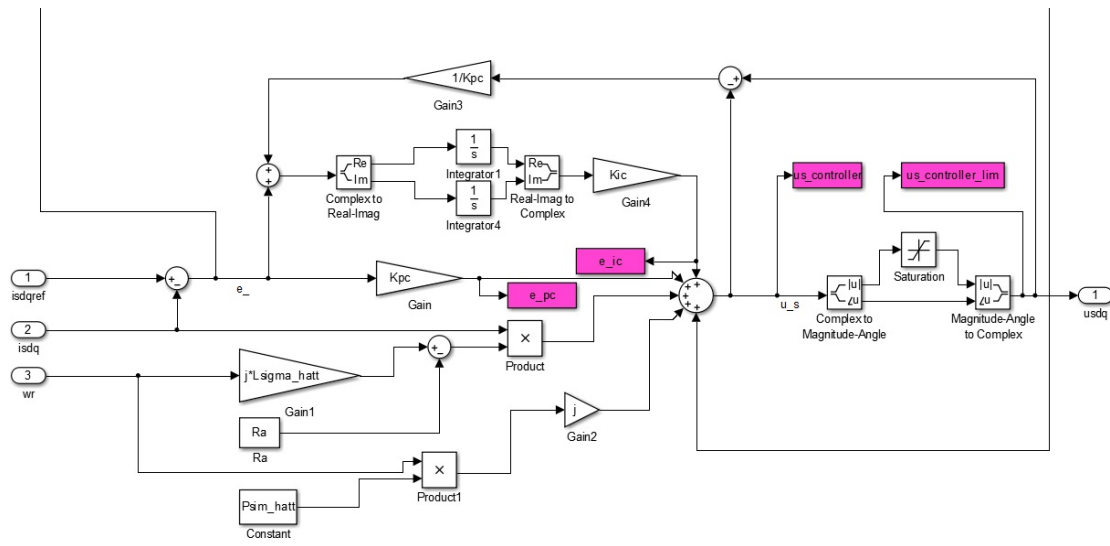


Figure 5.2: Current controller implemented in simulink

The resonant controller derived in Chapter 2.3.2 is visualised in Figure 5.3.

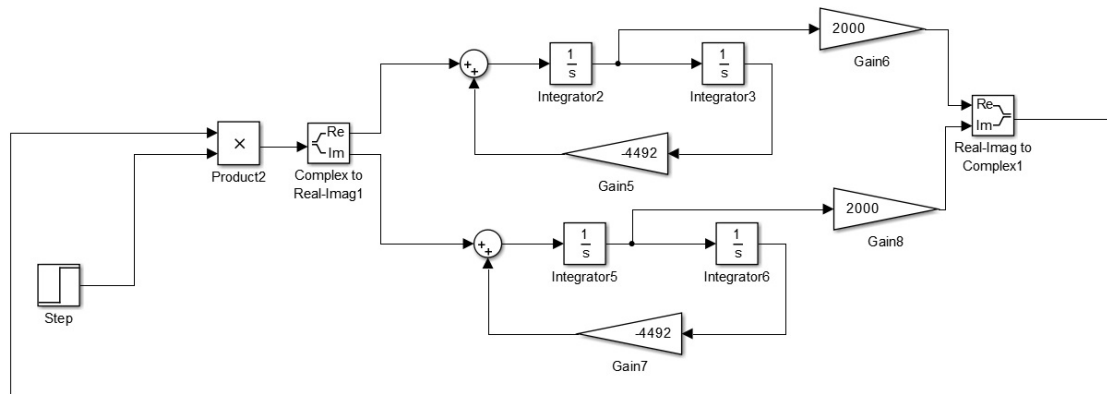


Figure 5.3: Resonant controller implemented in Simulink

5.1.3 Speed controller

In order to set up the simulations in a simpler way, an outer speed control loop is used to provide the torque reference to the current controller. This gives the possibility to

simulate the system both as a generator and a motor in an easy way.

5.2 Simulations

Simulations were done in order to investigate the behaviour of the machine during a start up of the machine and during open circuit fault conditions in the inverter.

5.2.1 Torque response

The simulation model was given a speed reference, with a low torque limit, to act similarly as the machine when it is given torque references manually.

5.2.2 Three-phase reference

In addition to this samples from normal three-phase operation was taken as reference. Up until this point the same dSpace controller as was used in the characterization was used. In order to create a better overview and provide easier modification possibilities a new controller was created in Simulink using Simulink RTI, a real time interface enabling interaction with dSpace.

5.2.3 Two-phase PI-control

Two-phase operation using only the PI-controller, Section 2.3.1, was achieved by manually forcing the current derivative of one phase in the machine model to zero. Moreover, the output from the machine model block was also forced to zero, in order to avoid that model outputs a DC value instead of zero, when turning the derivative of the current to zero. The current from the wye-point of the machine is not included in the model, but it is calculated manually in MATLAB, as $i_0 = -i_a - i_b$.

5.2.4 Resonant controller

The resonant controller can be attached to the system for the whole simulation, and reacts when the fault was introduced, however, in order to be able to first look at the faulty conditions, it is turned on a bit after the fault occurs. Also, the output of the resonant controller is analysed in order to use it as a reference for the validation as well.

6

Experimental test method

In this chapter the experimental test method is described and outlined. In the lab, verifications were made for a start up and continuously three phase running, as well as the open circuit phase fault with the resonant controller implementation.

6.1 Setup

For the experimental test the same lab setup, Figure 3.1, was used as is presented in Chapter 3 and was used for the characterisation in Chapter 4. The NewGen was driven as a motor for all tests with the induction machine disconnected and only acting as an external mechanical load.

6.2 Lab tests

The experiments described below are meant to verify the results from the machine characterisation and tests from the fault simulation.

6.2.1 Torque response

To verify the accuracy of the simulation model and the machine parameters acquired in Chapter 4, a start up test was performed in which the machine was accelerated with a torque reference of 325 Nm until it reached 21 rpm, where the torque was lowered to 275 Nm.

6.2.2 Three-phase reference

In addition to this, samples from normal three-phase operation was taken as reference. Up until this point the same controller as was used in the characterisation was used. In order to create a better overview and provide easier modification possibilities a new controller was created in Simulink RTI. The reference given to the machine was 275 Nm, which gave a speed of approximately 21 rpm.

6.2.3 Two-phase current control

Two-phase operation using only the original current controller, Section 2.3.1, was achieved by disconnecting phase C from the converter and connecting the wye-point in its place. Because of this arrangement, it was not possible to test the fault transition from three to two phase. Therefore, the machine was started with only two phases. The controller was configured to maintain the current from the wye-point to be the negative value of the two other phases added together, as shown in (2.24).

The controller as it was implemented in Simulink RTI is visualised in Figure 6.1.

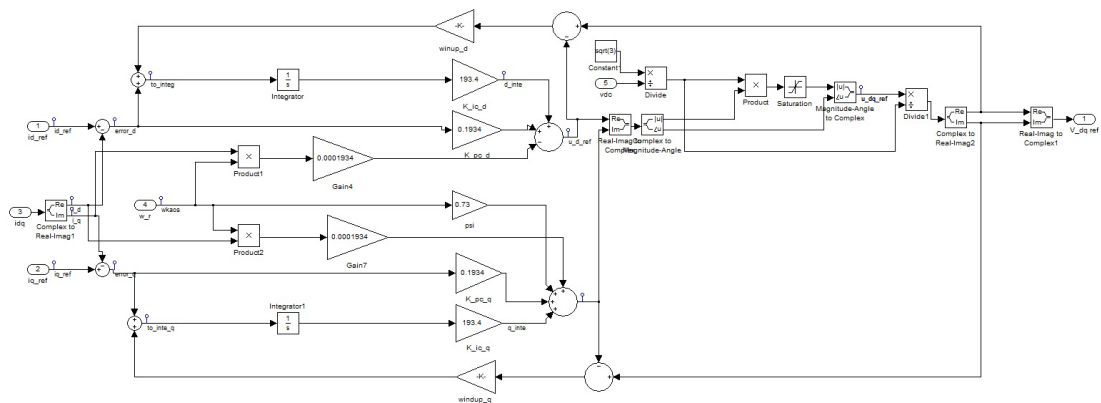


Figure 6.1: PI controller in Simulink RTI

6.2.4 Resonant controller

After two phase operation with the PI-controller was tested, the resonant controller as described in Section 2.3.2 was implemented in Simulink RTI as shown in Figure 6.2. Included in this setup was also a low pass filter, in order to reduce the influence of noise.

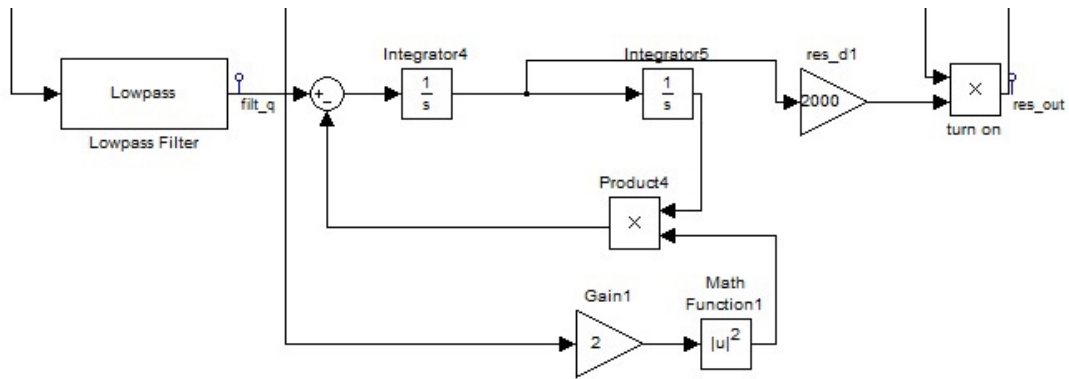


Figure 6.2: Resonant controller in Simulink RTI

6.2.5 Identifying sinusoidal component

Finally it was tested if a controller using the output of the simulated resonant controller and tuning it to the speed of the machine could improve on the torque ripple. This was implemented as a replacement to the resonant controller in Figure 6.2 and is presented in Figure 6.3.

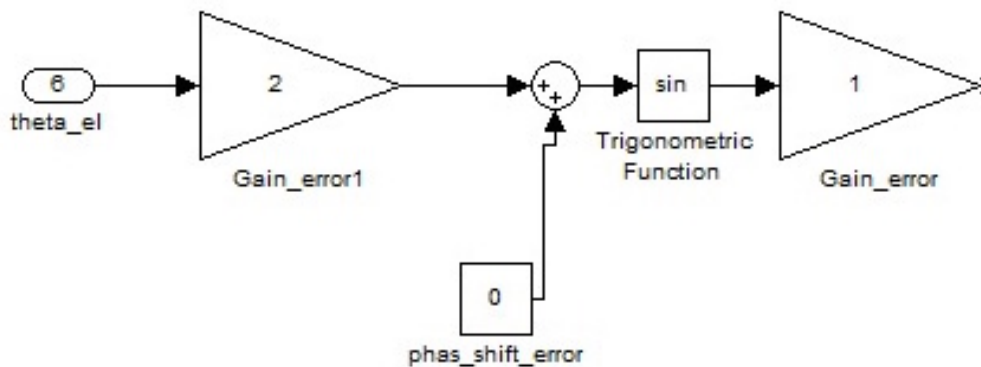


Figure 6.3: Introducing the response from the simulated resonant controller.

7

Results

The results includes both simulations and lab tests of the system. Firstly, the behaviour during a start up is presented, which verifies the Simulation model and the machine characterisation. Secondly, the behaviour during the open circuit phase fault is shown.

7.1 Model verification

The model is verified with both a simulation and lab tests. The results from both simulations and lab tests are what as expected, and they can be compared to each other.

7.1.1 Simulation

In the simulation a speed reference of 21.5 rpm was given to the machine, and the torque is limited to 325 Nm, in order to get a similar behaviour as in the lab.

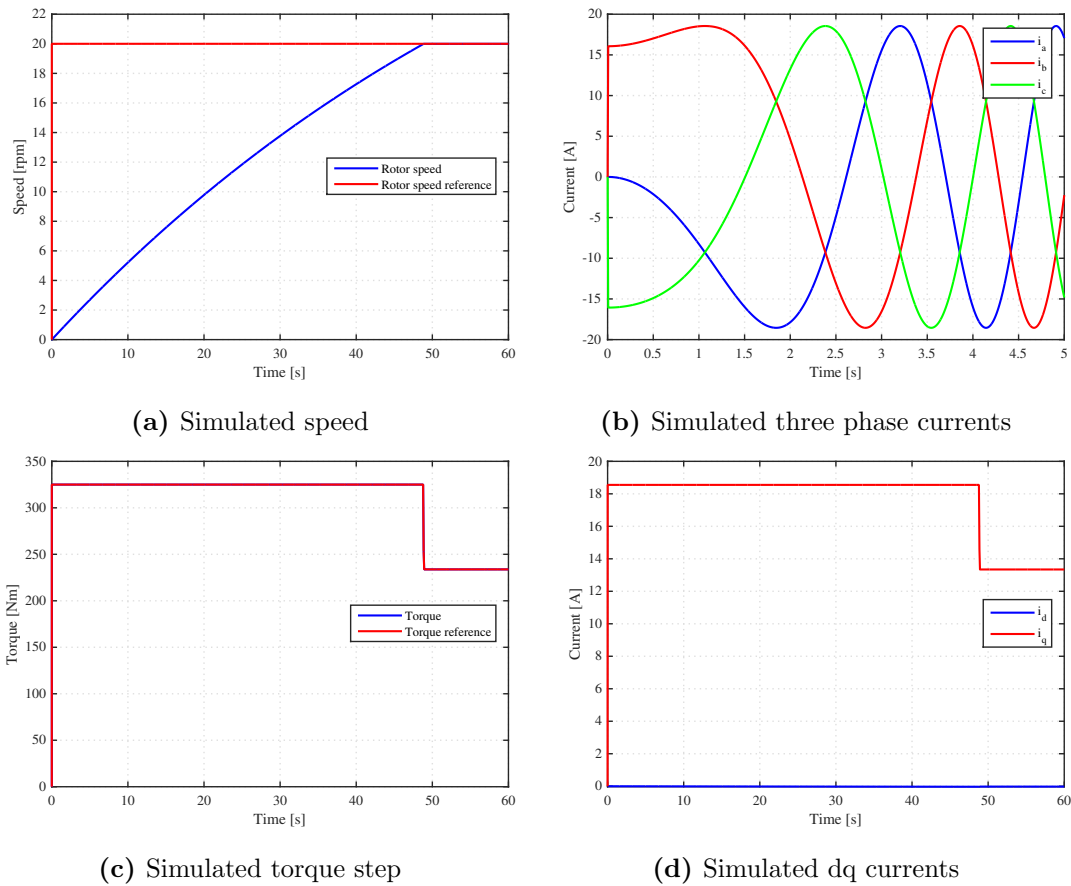


Figure 7.1: Simulation of start behaviour, speed reference

7.1.2 Lab verification

To confirm the simulations and the controller a torque reference was given to dSPACE, and the following results was obtained. However, there are some small differences. The speed does not reach 21.5 rpm, and the currents does not decrease as in the simulations. This is mainly due to that there was a speed regulator in the simulations, and only torque control in the lab test. Also, the gear box which is fitted to the machine is varying a lot in resistance, due to temperature.

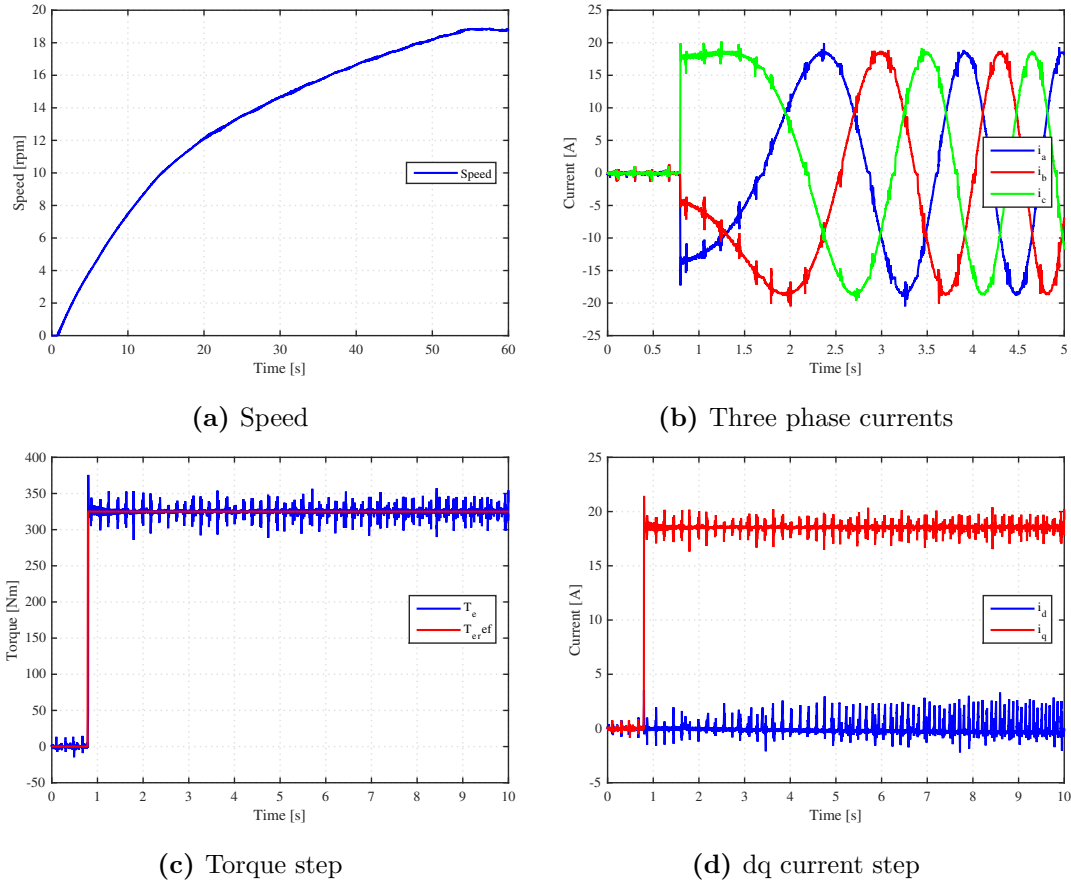


Figure 7.2: Validation of torque response

7.2 Open circuit phase fault

Both simulations and lab verifications were done for open circuit phase faults, in order to study the behaviour and try to implement the resonant controller for both cases, simulations as well as in the real drive system.

7.2.1 Simulations

The simulation was done at steady state conditions, and the results are given in Figure 7.4. In the simulations, the results shows three sequences, first healthy three phase performance between second five and six, then the fault is introduced and can be seen between second six and seven and the third part is when the resonant controller is turned on, from second seven to eight. From the simulations it can be seen that the resonant

controller has the capability to take care of the oscillating part which occurs during the outage of one phase, and gives a steady torque and current.

The frequency of the oscillations in the torque and current are as mentioned in Section 2.3.2 two times the electrical frequency of the machine, for 21 rpm, 11 Hz.

Furthermore, when one phase is gone, the two remaining phases has to give more current in order to maintain the same torque. This may be a problem when the machine is working on rated power, as the currents then will cause higher copper losses. Therefore, when working at rated power, the torque may need to be limited. In this particular case, the currents are small compared to the reted current of the machine, and no limitations are needed.

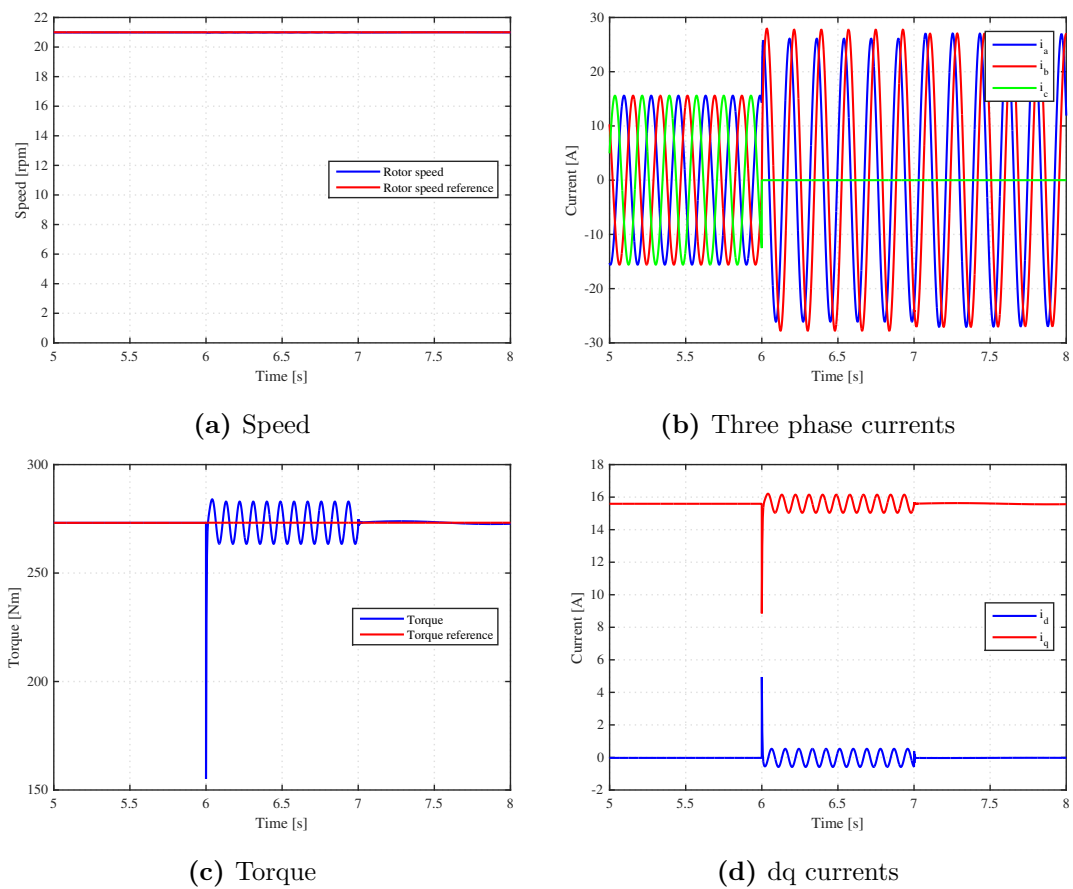


Figure 7.3: Simulated behaviour during resonant controller turn on

The output of the resonant controller in the simulations is shown in Figure 7.4a.

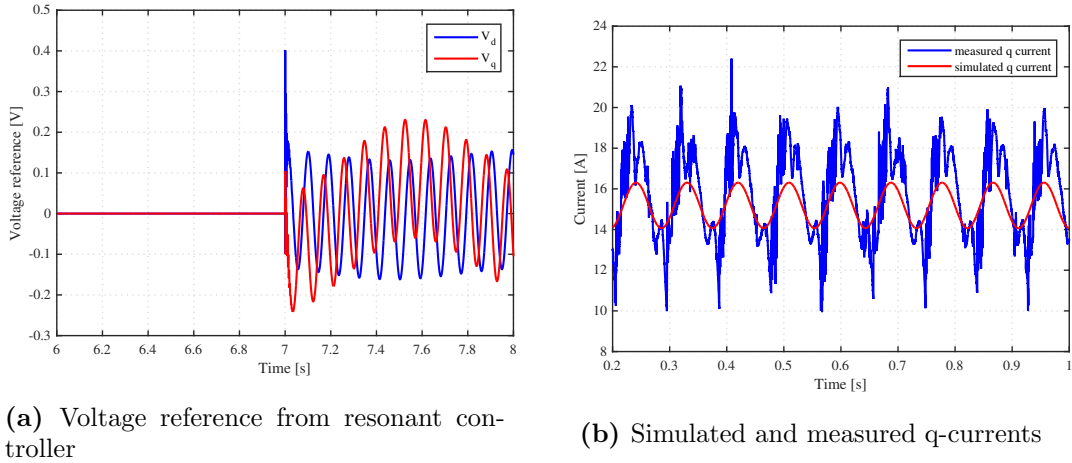


Figure 7.4: Simulated behaviour during resonant controller turn on

7.2.2 Identifying sinusoidal component

The q-currents during the open circuit fault for both the simulation and lab test are shown in Figure 7.4b.

From 7.4b, it can be seen that the double frequency component is present in both the simulation and in the lab tests. However, the measurement is distorted. Those distortions are also present before starting the machine, which can be seen the first second in 7.2.

7.2.3 Lab tests

Lab tests of the fault in the test set up was done when the machine was running at almost 21 rpm. After measurements was started, the resonant controller was activated in manually, multiplied with a constant in order to start by just a small part of the reference signal from the resonant controller.

The first implementation of the resonant controller in Simulink RTI was not very successful. As the resonant controller includes a derivative term, the distortion in the system, which can be seen in Figure 7.5d, which gave a very large oscillating reference from the resonant controller.

To improve the results from the resonant controller the input into the controller was filtered using a software low pass filter in Simulink RTI. However, the noise was taken away, but low frequency noise from the measurement was still found in the signals, making it hard to use the resonant controller, as the current still made steep changes.

As the resonant controller could not be implemented, due to steep changes in the measured current, the output from the resonant controller in the simulations were further investigated. From Figure 7.4b, it can be seen that the behaviour of the oscillations are the same in both the simulation and the lab tests.

Instead of the resonant controller, a similar reference signal as the reference from the simulated resonant controller was added to the system, and the results are given in Figure 7.5. The extra reference signal is given after 5.4 s, and as the torque depends only on the q-current, it is only implemented for the q-current.

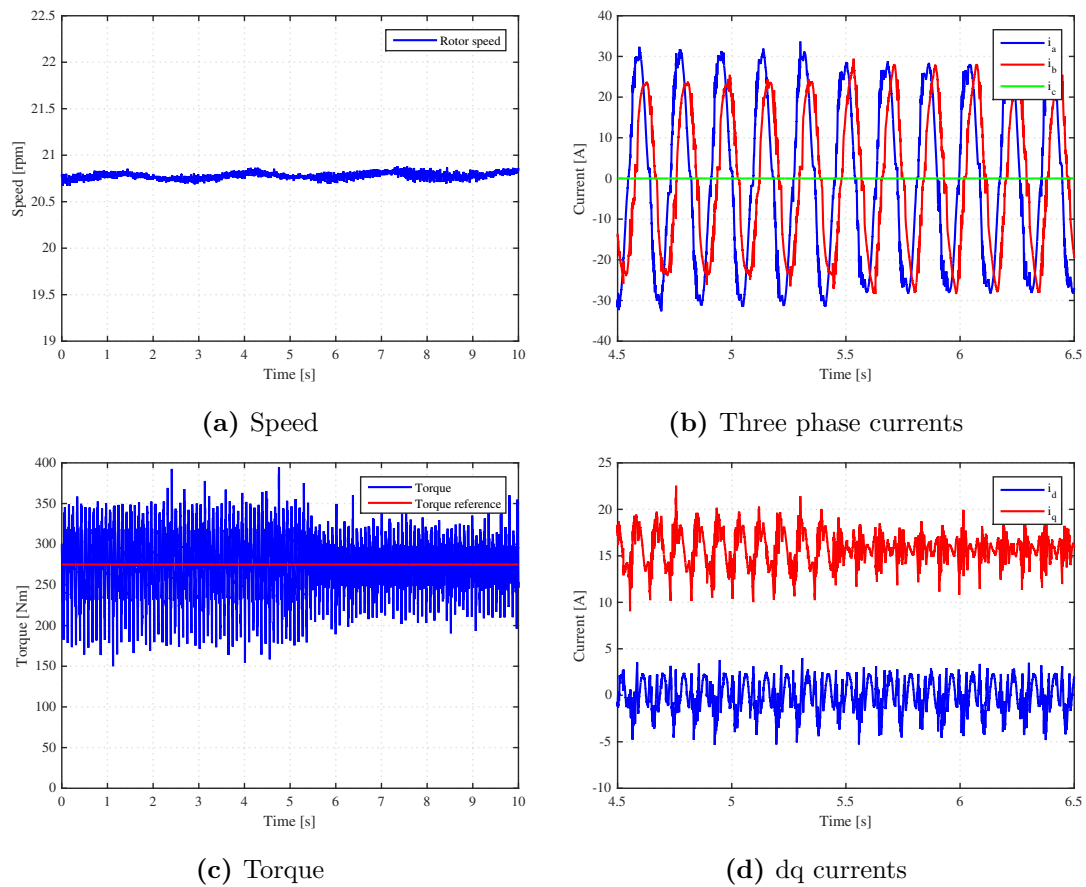


Figure 7.5: Behaviour during resonant controller turn on

From Figure 7.5 it can be seen that the added part, from the simulations does help the system in order to get more stable, and the oscillations are compensated for. The remaining noise is probably due to the converter and measuring.

8

Discussion

The parameters from the characterization gave a very accurate simulation model as seen in the start up test. Speed and current amplitudes corresponded well between simulation and experimental test. The main difference was that the currents in the experiment carried noise which resulted in an oscillating torque. The frequency of the oscillations was too high to have any consequences for the speed of the machine.

The simulation when using a PI-controller and implementing the fault worked well and turned out as expected. The speed was kept constant and controlling the current from the wye node resulted in a phase shift of the phase A and B currents, $+30^\circ$ and -30° respectively which manages to keep a rotating magnetic field. However the different amplitudes of the currents does give the field a slightly elliptic shape which results in a torque ripple with a frequency twice the electrical frequency of the machine.

When two-phase operation was tested in the lab the result was the same as in the simulations, with added noise. The sinus shape of the speed is a result of the encoder mounting as described in Section 3.3 and shows that the offset caused by the swing arm and non-centred axis is not fully compensated. When observing the d and q currents a clear sinus shape can be observed which has a frequency double that of the electrical frequency, the same as was seen in the simulation. This causes the torque reference to be likewise sinus shaped, however, the speed of the machine is not effected in any measurable way. This is likely due to the large inertia of the machine. Another machine with less inertia operating at higher speed would see more speed oscillations when using only two phases.

Implementing the resonant controller in the simulation model worked well. As seen in Figure 7.3d and 7.5d the oscillations on the d and q currents are completely removed when the resonant controller is engaged. In Figure 7.3b and 7.5b it can be seen that the A and B currents have the same amplitude after the introduction, resulting in a circular rotating magnetic field and thus a stable torque.

The experimental implementation did present major issues. The resonant controller contains a derivative term which means high frequency noise entering the controller will result in the output from the derivation being extremely high due to the steepness of the oscillation. This in combination with the integration results in an output from the resonant controller that increases with every iteration.

The obvious solution was to add a low pass filter to the input of the resonant controller in the dSpace/Simulink controller. This greatly reduced the output amplitude of the controller but presented other difficulties. The filter removed most of the noise which would have solved the problem with the derivation if the noise only originated in measurement error. Instead, using the filter resulted in the converter tripping due to the error signal being too large. What probably happened was that the noise was not entirely caused by the current measurements, meaning the low pass filter removed some noise that was actually present on the current, giving the resonant controller a false view of the current.

By observing the output of the simulated resonant controller, Figure 7.4b, it could be seen that it counteracted the sinus shape of the d and q current by adding a 90° phase shifted sinus of the same amplitude and frequency. Using this information it was possible to create a look-up table using the speed of the machine and implementing it in the dSpace/Simulink controller in place of the resonant controller, Figure 6.3. This counteracted most of the sinus shaped variations in the d and q currents. The A and B phase currents were controlled to the same amplitude giving a smoother torque, Figure 7.5.

9

Conclusion

Characterising the machine and using the parameters to create an accurate simulation model was successful. Operating the machine during an open circuit phase fault by controlling the current from the wye-node of the machine was also successful, with the expected drawback of current and consequently torque ripple.

Implementation of a resonant controller in the simulations gave a significant reduction of the current and torque ripple. It was not possible to implement the resonant controller in the physical system, as it includes a derivative term, resulting in very high output signals from the controller causing the converter to trip. However, replacing the resonant controller with a sinus shaped signal with the same amplitude as the main current oscillation and phase shifted 180° reduced the ripple significantly, showing the theoretical application of the controller to be helpful but with major difficulties in practical implementation. If the issues with the current noise could be solved the resonant controller is considered to be very useful in reducing current ripple and improving performance in case of open circuit faults.

9.1 Further research

When continuing the research presented in this thesis it is of utmost importance to solve the issue with high frequency, steep noise on the current. Simply using a SW LP-filter did not suffice. The next step would be to implement a HW LP-filter on the output of the converter. More extensive diagnostics to determine the cause of the noise is also desirable.

This thesis has had its main focus on the three-phase side of the converter, investigating the behaviour of the asymmetrical output, its effect on the machine and ways of counteracting the issues presented. It could be of interest to investigate the system in a wider perspective including the DC-side of the converter and possible effects. In an automotive

context the DC-side would be connected to a battery and the electrical system of the vehicle. Closer to this particular thesis might be the power generation sector since the NewGen is intended for use in wind turbines. PMSM's in wind power connections are often used in back-to-back converter systems where the power is transmitted via a DC-link through the tower of the plant and there converted to AC with grid frequency. Therefore the next step in investigating the use of resonant controllers in case of open circuit faults could be to evaluate its effect on the stability and behaviour of the DC-link.

Furthermore, additional further work would also include an investigation of other methods to handle the asymmetrical currents than the resonant controller.

Bibliography

- [1] B. Hernnäs, Direkt driven pilotgenerator, slutrapport, Tech. Rep. 02-2181:14, VG Power AB (2004).
- [2] Y. kang Chin, A permanent magnet synchronous motor for and electric vehicle - design analysis, Ph.D. thesis, Royal institute of technology (2004).
- [3] O. Wallmark, On control of permanent magnet synchronous motors in hybri electric vehicle applications, Ph.D. thesis, Chalmers University of Technology (2004).
- [4] Products, services for wind turbines, Electrical drivetrain solutions and products for turbine subsystems, ABB (2010).
URL [http://www05.abb.com/global/scot/scot234.nsf/veritydisplay/ad5bbdf249b6d94ec125784f0037fe77/\\$file/products_and_services_for_wind_turbines_lowres.pdf](http://www05.abb.com/global/scot/scot234.nsf/veritydisplay/ad5bbdf249b6d94ec125784f0037fe77/$file/products_and_services_for_wind_turbines_lowres.pdf)
- [5] S. K. Bisoyi, R.K.Jarial, R.A.Gupta, Modeling and control of variable speed wind turbine equipped with pmsg, International Journal of Emerging Technologies in Computational and Applied Sciences 13 (513).
- [6] E. Eitel, The difference between ac induction, permanent magnet, and servomotor technologies.
URL <http://machinedesign.com/motorsdrives/difference-between-ac-induction-permanent-magnet-and-servomotor-technologies>
- [7] P. Sekerák, V. Hrabovcová, P. Rafajdus, L. Kalamen, M. Onufer, Effect of permanent magnet rotor design on pmsm properties, Transactions on Electrical Engineering 1 (3).
- [8] J. Härsjö, Modeling of pmsm full power converter wind turbine with turn-to-turn fault, Ph.D. thesis, Chalmers University of Technology (2014).
- [9] N. Phung Quang, J.-A. Dittrich, Vector Control of Three-Phase AC Machines, Springer, 2008.

- [10] S. Bolognani, M. Zordan, M. Zigiolotto, Experimental fault-tolerant control of a pmsm drive, *IEEE Transactions on Industrial Electronics* 47 (5) (2000) 1134–1141.
- [11] Y. Crévits, X. Kestelyn, E. Semail, Investigation on vector control of three-phase synchronous machines under supply fault conditions, *International Symposium on Power Electronics, Electrical Drives, Automation and Motion*, 2006.
- [12] C. Du-Bar, Design of a fault-tolerant fractional slot pmsm for a vehicle application, Ph.D. thesis, Chalmers University of Technology (2015).
- [13] S. Engström, The newgen direct drive generator for large wind turbines, Tech. rep., NewGen Generator AB (2011).
- [14] Semikron, SKM 300GB125D Ultra fast IGBT Module (2009).
- [15] dSPACE GmbH, Technologiepark 25 33100 Paderborn, Germany, Hardware Installation and Configuration, 6th Edition (2009).

A

Equipment setup

In this chapter the equipment used in the complete system as shown in Figure A1 is presented, including measurement equipment.

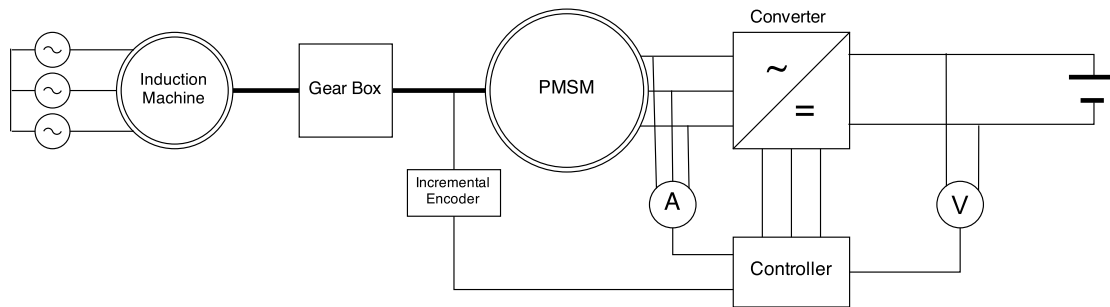


Figure A1: System setup

A.1 Test object PMSM

The machine used in the tests was a NewGen, Chapter 3.1, specifically a prototype machine developed for tests of the general principle. The machine parameters as given by the developer are displayed in Table A1.

Table A1: Machine parameters [1].

General		Rotor	
Rated apparent power, (S_n)	144 kVA	Rotor outer diameter	1798 mm
Maximum apparent power, (S_{max})	177 kVA	Rotor inner diameter	1650 mm
Rated current, (I_n)	616.8 A	Stator	
Power factor, (ϕ)	1	Stator outer diameter	1600 mm
Open circuit voltage, (V_{OC})	151.3 V	Stator inner diameter	1300 mm
Load voltage, (V_{load})	131.0 V	Stator axial length	140 mm
Rated speed, (ω_n)	100 rpm	Air gap (min)	4 mm
Number of pole pairs (np)	16	Number of winding slots	168

A.2 Induction machine

Asea MEK 250 S-4 Asynchronous machine.

Table A2: Induction machine technical data.

Rated apparent power (S_n)	87 kVA
Rated current (I_n)	126 A
Load voltage (V_{load})	400 V
Rated speed (ω_n)	1540 rpm

A.3 Converter

A.4 Gearbox

Rademakers Rotterdam RAWE.PLAN.PIF.05 gearbox

Table A3: Gearbox technical data.

Ratio	1:19.85
Rated speed	75/1500 rpm
Maximum power transfer	40 kW

A.5 dSpace

A.6 Measurement equipment

A.6.1 Position sensor

Hengstler Rotary incremental encoder 5000, RI58-O/5000AS.41RB.

Table A4: Encoder technical data.

Pulses	5000
Output	RS 422
Operating voltage	5 VDC
Connection	Cable, 1.5 m, radial
Revolution speed	max. 10000 rpm
Operating temperature	-10...+70 °C
Protection rating	IP65
Dimensions d x L	58 x 41.5 mm
d shaft	6 mm
Pulse frequency	max. 300 kHz
Shaft load capacity	40 N radial, 20 N axial
Housing material	Aluminium

A.6.2 Oscilloscope

LeCroy WaveSurfer 24MXs-B Oscilloscope.

Table A5: Oscilloscope technical

Vertical system		Horizontal system	
Rise time	1.75 ns	Time/	200 ps/div -
Bandwidth	200 MHz	Division range	1000 s/div
Input channels	4	Clock accuracy	5 ppm
Bandwidth limit	20 MHz	Trigger, interpolator jitter	3 ps (rms)
Sensitivity	1 M Ω : 2 mV/div - 10 V/div 50 Ω : 2 mV/div - 1 V/div		
DC gain accuracy	$\pm 1.5\%$ ± 1 V: 2 mV/div - 99 mV/div		
Offset range	± 10 V: 100 mV/div - 1.0 V/div ± 100 V: 1.02 V/div - 10 V/div		

A.6.3 Current sensors

LeCroy CP150 Current Probe

Table A6: Current probe.

Bandwidth	10 MHz
Coupling	AC 1 M Ω , DC 1M Ω , GND
Risetime (typical)	35 ns
Max continuous input current	150 A
Max Peak Current	300 A
Minimum Sensitivity	100 mA/div
Amplitude accuracy	$\pm 1.0\%$ of reading ± 100 mA to 150A $\pm 2.0\%$ of reading to 300A

A.6.4 Voltage probes

LeCroy AP032 Differential Probe

Table A7: LeCroy AP032 voltage probe.

Bandwidth	25 MHz
Rise time	14 ns
Attenuation	1:20/1:200
Atten. accuracy	$\pm 2\%$
Input resistance	4 $M\Omega$
Input capacitance	10 pF each side to ground
Output offset (typical)	$< \pm 5$ mV
Output noise	1.5 to 2 mV

t